Fully coupled atmospheric-hydrological modeling at regional and long-term scales: Development, application, and analysis of WRF-HMS

Sven Wagner, Benjamin Fersch, Fei Yuan, Zhongbo Yu, Harald Kunstmann

Angaben zur Veröffentlichung / Publication details:

Wagner, Sven, Benjamin Fersch, Fei Yuan, Zhongbo Yu, and Harald Kunstmann. 2016. "Fully coupled atmospheric-hydrological modeling at regional and long-term scales: Development, application, and analysis of WRF-HMS." *Water Resources Research* 52 (4): 3187–3211. https://doi.org/10.1002/2015wr018185.

AGU PUBLICATIONS

Water Resources Research

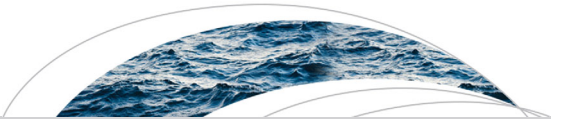

RESEARCH ARTICLE

10.1002/2015WR018185

Key Points:
- Development of a fully coupled hydro-meteorological modeling system extending WRF with HMS
- Implementation of two-way groundwater-unsaturated zone interaction in the Noah-LSM of WRF
- Model system application and investigation of the impact of coupling for Poyang Lake basin, China

Correspondence to:
S. Wagner,
sven.wagner@kit.edu

Citation:
Wagner, S., B. Fersch, F. Yuan, Z. Yu, and H. Kunstmann (2016), Fully coupled atmospheric-hydrological modeling at regional and long-term scales: Development, application, and analysis of WRF-HMS, *Water Resour. Res.*, *52*, 3187–3211, doi:10.1002/2015WR018185.

Received 2 OCT 2015
Accepted 23 MAR 2016
Accepted article online 29 MAR 2016
Published online 29 APR 2016

Fully coupled atmospheric-hydrological modeling at regional and long-term scales: Development, application, and analysis of WRF-HMS

Sven Wagner[1,2], Benjamin Fersch[1], Fei Yuan[3], Zhongbo Yu[3], and Harald Kunstmann[1,2]

[1]Institute of Meteorology and Climate Research, Karlsruhe Institute of Technology, Garmisch-Partenkirchen, Germany, [2]Institute of Geography, University of Augsburg, Augsburg, Germany, [3]State Key Laboratory of Hydrology-Water Resources and Hydraulic Engineering, Hohai University, Nanjing, China

Abstract A closed description of the regional water balance requires hydro-meteorological modeling systems which represent the atmosphere, land surface, and subsurface. We developed such a mesoscale modeling system, extending the atmospheric model WRF with the distributed hydrological model HMS in a fully coupled way. It includes explicit lateral groundwater and land surface flow parameterization schemes and two-way groundwater-unsaturated zone interaction by replacing the free drainage bottom boundary of WRF's Noah-LSM with a Fixed-head or Darcy-flux boundary condition. The system is exemplarily applied for the Poyang Lake basin (160,000 km^2) and the period 1979–1986 using a two-nest approach covering East Asia (30 km) and the Poyang Lake basin (10 km) driven by ERA Interim. Stand-alone WRF effectively simulates temperature (bias 0.5°C) and precipitation (bias 21–26%). Stand-alone HMS simulations provide reasonable streamflow estimates. A significant impact on the regional water balance was found if groundwater-unsaturated zone interaction is considered. But the differences between the two groundwater coupling approaches are minor. For the fully coupled model system, streamflow results strongly depend on the simulation quality for precipitation. Two-way interaction results in net upward water fluxes in up to 25% of the basin area after the rainy season. In total, two-way interaction increases basin averaged recharge amounts. The evaluation with CPC and GLEAM indicates a better performance of the fully coupled simulation. The impact of groundwater coupling on LSM and atmospheric variables differs. Largest differences occur for the variable recharge (26%), whereas for atmospheric variables, the basin-averaged impact is minor (<1%). But locally, a spatial redistribution up to ±5% occurs for precipitation.

1. Introduction

On all scales, the components of the hydrologic cycle change continuously and affect the availability and quality of water as essential prerequisites for human development and sustainable ecological conditions. Climate and land use changes are thereby the main drivers for changes in the hydrologic cycle. Feedback mechanisms within the hydrologic cycle play a crucial role for a rational quantification of past, current, and future water availability. Dynamic feedback among the compartments is primarily connected to the water and energy fluxes between the subsurface, land surface, and atmosphere and is inextricably intertwined over a large range of spatiotemporal scales.

In atmospheric modeling, land surface models (LSMs) form the lower boundary condition for the atmosphere to parameterize subgrid scale land surface processes, in particular water and energy fluxes. Most commonly, LSMs in atmospheric modeling are one-dimensional column models describing the interactions of the atmospheric boundary layer, the vegetation, and the soil. Coupled atmospheric-hydrological modeling systems additionally include lateral water fluxes at the surface and groundwater processes with or without feedback to the LSM. The investigation of these feedback mechanisms has motivated recent efforts in coupled land surface-hydrological and atmospheric-land surface-hydrological modeling systems for different spatial and temporal scales.

Several studies have investigated the interaction between groundwater table dynamics and land surface fluxes by coupling LSMs with groundwater models [e.g., *Yeh and Eltahir*, 2005; *Maxwell and Miller*, 2005; *Kollet and Maxwell*, 2008; *Zeng and Decker*, 2009; *Rosero et al.*, 2009]. *Kollet and Maxwell* [2008] examined the

influence of groundwater dynamics on the energy and mass balances at the land surface by integrating the Common Land Model (CLM) into ParFlow, a variably saturated 3-D groundwater flow model with integrated overland flow capabilities. For the Little Washita watershed (600 km^2) in Oklahoma, USA, they found reasonable agreement between simulation results and observations, and a strong interconnection between components of the energy cycle and groundwater if the groundwater level is within a critical depth. For the same catchment, *Rosero et al*. [2009] investigated the performance of the unified Noah-LSM and a hydrologically enhanced Noah-LSM with a simple aquifer model and topography-related surface and subsurface runoff parameterizations on simulating the water cycle. *Zeng and Decker* [2009] suggested to replace the free drainage bottom boundary condition used by many LSMs by a new lower boundary condition which is based on an equilibrium soil moisture distribution. This approach allows a coupling between groundwater and surface water. They implemented this method in the Community Land Model (CLM3.5) for global offline modeling evaluations and achieved improved performances.

Atmospheric-land surface-hydrological modeling systems were developed by, e.g., *Seuffert et al*. [2002] who coupled the TOPMODEL-Based Land Surface-Atmosphere Transfer Scheme (TOPLATS) with the operational German weather forecast model LM (Lokal Modell) to investigate the influence of a land surface hydrologic model on the predicted local weather. *York et al*. [2002] coupled a single-column atmospheric model with a distributed soil-vegetation-aquifer model to study aquifer-atmosphere interactions in watersheds on decadal time scales. *Maxwell et al*. [2007] combined ParFlow and the mesoscale atmospheric model ARPS to examine the effects of soil moisture heterogeneity on atmospheric boundary layer processes. They showed for idealized test cases that the fully coupled model maintains a realistic topographically driven soil moisture distribution and depicts spatial and temporal correlations between surface and lower atmospheric variables and water table depth. *Maxwell et al*. [2011] coupled ParFlow with WRF via the Noah-LSM. They demonstrated that the more precise runoff mechanisms and lateral water flows change the spatial patterns of land surface-atmosphere fluxes in idealized simulations. *Shrestha et al*. [2014] presented a scale-consistent terrestrial systems modeling platform (TerrSysMP) consisting of the atmospheric model COSMO, the land surface model CLM, and ParFlow coupled with the external coupler OASIS. In addition to idealized simulations, they performed short-term real data simulations for the Rur catchment in Germany (150 km $\times$ 150 km). The TerrSysMP simulation produced slightly improved land surface-atmosphere flux predictions and indicated a strong sensitivity to initial soil moisture conditions. *Gochis et al*. [2013] developed the WRF-Hydro model coupling extension package which connects hydrological model components with atmospheric models. Here a distributed surface, a channel routing, and a groundwater module are implemented. For a more detailed description of the lateral flows at the land surface, the computation of surface and streamflow routing is performed on a higher-resolution subgrid. A dynamically coupled climate-hydrological modeling system using the RCM HIRHAM and the hydrological model MIKE-SHE was developed by *Butts et al*. [2014]. The model system was applied for the 2500 km^2 Skjern River catchment, Denmark, for a 14 months simulation. They found only small differences in net precipitation and catchment runoff for this single hydrological year and stated the need for long-term, decadal simulations. With the same modeling system and for the same catchment, *Larsen et al*. [2014] investigated the impact of the data transfer interval between the RCM and the hydrological model on simulation results.

Atmospheric-hydrological modeling systems using three-dimensional variably saturated surface and subsurface flow models (e.g., ParFLOW) or high-resolution subgrids for surface and streamflow routing (e.g., WRF-Hydro) are in general very CPU-intensive. Therefore, many of the recent studies were performed with idealized simulations or relatively small watersheds or relatively short time periods. For larger-scale applications on incorporating water table dynamics in climate modeling, *Miguez-Macho et al*. [2007] introduced groundwater process description in the Regional Atmosphere Modeling System (RAMS). They expanded the land surface model LEAF2 to include groundwater and rivers-lakes reservoirs. Using this coupled regional climate-hydrologic modeling system RAMS-Hydro, *Anyah et al*. [2008] investigated the role of the water table dynamics on soil moisture and atmospheric fluxes for North America for the warm season 1997 with a spatial resolution of 50 km (12.5 km) for the atmosphere (land). *Jiang et al*. [2009] used the WRF model coupled with an augmented Noah land surface model which includes an interactive canopy model and a simple groundwater model (SIMGM) [*Niu et al*., 2007]. They performed experiments for the summer season 2002 over the entire United States with 32 km horizontal resolution. They showed that incorporating vegetation and groundwater dynamics into WRF produces more precipitation, which improves the simulation of

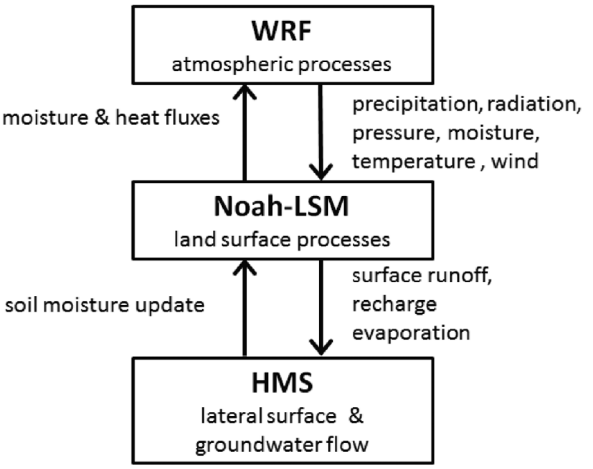

Figure 1. Schematic diagram of the fully, two-way coupled regional atmospheric-hydrological model system.

summer precipitation over the Central U.S. For the East Asian monsoon region, *Yuan et al*. [2008] investigated the effects of water table dynamics on regional climate. They found a reduction of systematic bias of simulated precipitation in the summertime of 2000. They concluded that dynamical representation of groundwater in a RCM affects convection due to changes in the vertical profile of soil moisture and therewith the surface moisture and heat fluxes, which results in different structures of the boundary layer.

This literature review shows that depending on the research question and spatial scale, several coupled atmospheric-hydrological model systems have been developed which differ in their complexity. Modeling systems with three-dimensional variably saturated subsurface and integrated surface runoff are particularly applied for smaller watersheds and/or short-term periods due to their computational demands. For macroscales (e.g., continental scale) investigations, less complex model systems were developed which mainly focus on the coupling of groundwater to the LSM.

The goal of this study is to develop a model system with a closed description of the water cycle on regional and long-term scales. For this purpose, standard regional atmospheric models require a more detailed description of the complex hydrological processes at the land surface and subsurface. In particular, lateral groundwater flow and interactions between saturated zone, unsaturated zone, and lake or river water are important processes which are usually not considered in standard regional atmospheric models. To account for this, we have developed such a fully two-way coupled, atmospheric-hydrological model system by combining the regional atmospheric model WRF-ARW [*Skamarock et al*., 2008] with the distributed hydrological model HMS [*Yu et al*., 2006]. This coupled system can be applied for long-term simulations at climate-relevant scales for multiple years and longer time periods for mesoscale to large-scale river catchments. Hence, this model system enables in particular investigations of regional and long-term interactions among groundwater, soil moisture dynamics, and the atmosphere. It allows to study the impact of groundwater coupling on the conditions at the land surface and the lower atmosphere. The performance and ability of the closed description of the regional water cycle with this fully coupled atmospheric-hydrological model system is demonstrated for the Poyang Lake basin (160,000 km^2) in South China. The basin, which is an important flood storage area for the Yangzte River, comprises the largest freshwater lake in China and is prone to severe floods and droughts.

In section 2, a description of the models, the coupling strategy, and the implementation of the two-way interaction between groundwater and Noah-LSM are presented. The Poyang Lake basin, the study area of the first application of the coupled model system, is introduced in section 3 together with the forcing and validation data sets and the simulation design. In section 4, the performances of stand-alone WRF and HMS simulations are presented. Furthermore, the impact of groundwater coupling on the stand-alone HMS results is elaborated. Finally, the performance and potential of fully coupled WRF-HMS simulations are investigated and evaluated along with hydro-meteorological observations. The results are summarized and concluded in section 5.

2. The Coupled Model System

A schematic diagram of the fully, two-way coupled atmospheric-hydrological model system is displayed in Figure 1. It depicts the applied models and the variables which are transferred between the atmospheric, land surface, and hydrological models. In general, LSMs require surface meteorological data and provide surface runoff, evapotranspiration, and recharge to the hydrological model. In a fully coupled application,

the hydrological part of the simulation may result in an altered soil moisture distribution, which is returned to the LSM. Subsequently, the LSM provides heat and moisture fluxes to the atmospheric model. In this section, the components and the coupling method of this atmospheric-hydrological model system are briefly described.

2.1. WRF

For the atmospheric simulations, the Weather Research and Forecasting (WRF) model with the Advanced Research WRF (ARW) dynamics solver version 3.3.2 [*Skamarock et al*., 2008] is used. The WRF model is a non-hydrostatic, mesoscale numerical weather prediction, and atmospheric simulation system. It offers multiple physics options, which parameterize subgrid-scale physical processes, e.g., convection, microphysics, radiation, or the planetary boundary layer. Furthermore, LSMs compute heat and moisture fluxes over the surface acting as lower boundary for atmospheric models. Our setup uses the Noah-LSM [*Chen and Dudhia*, 2001]. It is a four-layer soil temperature and moisture model with canopy moisture and snow cover prediction. It explicitly solves vertical water flow, using the diffusive form of the Richards equation. For the calculation of subsurface runoff, which is defined as the drainage of the lowest soil layer of the LSM, a gravitational parameterization is used. For the calculation, the hydraulic conductivity is multiplied by a temporal constant slope factor between 0.1 and 1.0. The dependencies among soil hydraulic conductivity, water matric potential, and volumetric soil moisture are parameterized after *Clapp and Hornberger* [1978].

2.2. HMS

HMS is a spatially distributed hydrological model, developed for mesoscale and large-scale hydrological simulations [*Yu et al*., 2006]. HMS explicitly predicts unsaturated-zone soil moisture, river-vadose and river-groundwater exchange, streamflow routing, and lateral groundwater flow. For groundwater, a one-layer aquifer is assumed. The horizontal flow is expressed by the 2-D Boussinesq equation. In the vadose zone, a steady state soil moisture profile is assumed. Channel-vadose zone and channel-groundwater flow depends on the riverbed depth, hydraulic head, and surface water level. Surface water flows are formulated with a 2-D diffusive wave equation that includes river flow routing, lake depth and extent, and interaction between the surface water and subsurface water [*Yu et al*., 2006]. For the calculation of the water and energy fluxes at the land surface, *Yuan et al*. [2009] replaced the original implemented LSX-LSM with the Noah-LSM in HMS. Here the stand-alone HMS version is used for the observation-based calibration of the hydrological part of the fully coupled model system.

HMS was selected for the description of the hydrological processes in the coupled model system due to the following reasons: HMS is a spatially distributed model which was specifically developed for mesoscale and large-scale hydrological simulations using grid cells in the range of tens of kilometers. This implies identical horizontal grids of the atmospheric and hydrological model. Furthermore, both models are bound to the Noah-LSM and share compatible water and energy flux formulations.

2.3. WRF-HMS One-Way Coupling

The coupling of WRF and HMS enhances the representation of terrestrial hydrological processes in long-term regional dynamic climate simulations. For both models, WRF and HMS, the Noah-LSM can be used to simulate land surface processes (see sections 2.1 and 2.2). Hence, the Noah-LSM acts as the interface between the WRF and HMS model (see Figure 1).

The Noah-LSM considers single vertical columns of vegetation, snow, and soil at each grid cell over land without horizontal interactions between adjacent grid cells to calculate the water and energy fluxes at the land surface, soil moisture, and temperature profiles as well as surface and subsurface runoff. With the coupling of HMS, detailed hydrological processes such as river routing and discharge, river-vadose zone and river-groundwater exchange, lake extents and depths, and groundwater flow are explicitly included.

As described in *Yu et al*. [2006], HMS calculates two prognostic variables predicting the water amounts in each grid cell: the total amount of water in river and lakes (V_l) and the total amount below ground which includes groundwater plus vadose zone soil moisture (V_g). Therefore, HMS requires the following time-variant input data from the Noah-LSM: precipitation, potential evaporation, and surface and subsurface runoff. Precipitation and potential evaporation are used for the calculation of the water fluxes over lakes and large rivers which are required for the calculation of V_l. For the river routing and discharge calculation, HMS assumes, as most large-scale hydrologic models, that there is only one major river resolved for each grid

cell and that minor streams deliver local surface runoff from the Noah-LSM instantaneously to that river. The subsurface runoff results from the Noah-LSM are used as source term in the calculation of the water amount below ground (V_g) together with the horizontal groundwater flow by Darcy law and the channel-vadose and channel-groundwater interactions.

Technically, the HMS model is embedded into the WRF model system by a newly implemented hydrological driver. This driver routine controls time stepping and the temporal aggregation and passing of flux variables for the HMS invocation. To optimize computational efficiency, HMS can be invoked on a coarser time step than WRF, allowing to account for the lower temporal dynamics of the relevant hydrological processes on the mesoscale in comparison to atmospheric processes. In general, for regional applications, atmospheric models require modeling time steps in the range of tens of seconds to minutes, depending on the model resolution, whereas an hourly-to-daily time step might be sufficient for HMS.

Due to the computational requirements, atmospheric models are usually applied in parallel mode on high-performance computing clusters (HPC). Since the WRF model uses the Message-Passing-Interface (MPI) for parallelization, the HMS code was converted to be consistent with the modular FORTRAN90 formulation of WRF and adapted to support MPI parallel execution. For an improved workflow, the input and output sections of stand-alone HMS were converted to support the netCDF binary format. In addition, a conversion routine was needed to exchange the single precision floating point variables of WRF with the double precision variables of HMS. In our study, the additional computational demand compared to standard WRF simulations was approximately 20%.

The added-value of this one-way coupled model system is the enhanced description of hydrological processes by adding lateral flows and river-vadose and river-groundwater exchange processes. Furthermore, there is no redundancy as it is the case with offline coupling where the land-surface variables are calculated separately for each component, often with different land surface models.

The HPC capability of the coupled modeling system provides the basis for the long-term simulations that are performed for this study, i.e., multiyear or tens of years simulation runs.

2.4. WRF-HMS Two-Way Coupling With Groundwater Feedback

In addition to the coupling of atmospheric and lateral hydrological processes, two methods allowing for the interaction between the groundwater and soil moisture states of the LSM were implemented. By capillary rise, the groundwater table can affect the moisture content of the upper unsaturated zone and at the land surface, which in turn result in altered conditions for the exchange of water and energy between the atmosphere and land. This upward flux is often not taken into account in LSMs that are typically used in RCMs such as the Noah-LSM in WRF.

To investigate in particular the long-term interactions among groundwater, unsaturated zone, and atmosphere for large-scale river catchments, we have implemented two coupling approaches that enable the exchange of moisture between the lowest soil layer of the Noah-LSM and the saturated zone as a function of groundwater table depth.

One approach follows the methodology proposed by *Zeng and Decker* [2009] and the associated comment of *De Rooij* [2010]. Here the free drainage boundary condition of the LSM is replaced with a prescribed hydraulic head which allows an exchange of water in both directions across the bottom boundary of the LSM. The hydraulic head at the lower boundary of the LSM is derived from the distance between groundwater level and the bottom of the LSM, thereby conserving the energy and mass of the vertical water flux and assuming an equilibrium soil moisture profile. A set of equations to calculate average matrix heads and water contents for saturated, unsaturated, and partially saturated conditions are implemented. Technically, the new boundary condition is realized with an additional layer at the bottom of the Noah LSM. This method defines a Fixed-head boundary condition in the Richards equation and thus is referred to as *Fixed-head*, hereinafter.

The second approach used in this study is adopted from *Bogaart et al*. [2008]. They developed a computationally efficient parameterization that approximates the solution of the Darcy-Buckingham equation with respect to the LSM bottom layer moisture content, and the groundwater depth, assuming a quasi steady state moisture profile. Further details can be found in *Bogaart et al*. [2008] and in *Fersch et al*. [2013]. In the following, this method is denoted as *Darcy-flux*.

In addition to the upward transport of water from the saturated to the unsaturated zone, the implementation of the *Fixed-head* or *Darcy-flux* method increase the possible value range of recharge amounts in comparison to the free drainage boundary condition. Therefore, both methods also enable higher downward recharge amounts than the standard method.

3. A Water Budget Study for the Poyang Lake Region

3.1. Study Area

The developed coupled model system is exemplarily applied for the Poyang Lake basin (160,000 km^2) in South China. The Poyang Lake is the largest freshwater lake (4000 km^2) in China and the basin is prone to floods that regularly occur during the summer rainy season. It is connected to the main stream of the Yangtze River and therefore an important flood storage and detention area for the Yangzte River.

The watershed is situated south of the Yangtze River between 27°N–30°N and 115°E–118°E. This area is characterized by a humid subtropical climate and strongly affected by the East Asian monsoon. It has a mean annual air temperature of 17.6°C and an annual precipitation of about 1500 mm, with most of the rain falling between April and September. For the land use and soil classification in the WRF domains, the global data sets of the WRF preprocessing system WPS using USGS classification are used. For the Poyang Lake basin, the dominant land use types are irrigated cropland and pasture which covers approximately 40% of the total area and different forest types, mainly deciduous-broadleaf (20%), evergreen needle (10%), and mixed (4%) forest. The soil is mainly classified as clay-loam (60%) in the northern and central part of the basin and as clay (37%) in the South and the fringe area. The topography of the Poyang Lake basin is comparatively flat (see Figure 2c). The upper reach areas of the five rivers flowing into the Poyang Lake are characterized by mountainous area, the middle reaches by low hilly terrain, and the lower reaches by alluvial plain.

Due to the importance of the Poyang Lake basin as flood storage area and the severe floods and droughts in the past, several hydrological and climatological studies have focused on this basin. For example, *Shankman et al*. [2006] found that since 1950 the most severe floods in the Poyang Lake occurred during or immediately following El Nino events, which are directly linked to heavy rainfall in central China. The impact of significant changes in hydro-climatic variables and human activities on the changes of streamflow in the Poyang Lake basin between 1960 and 2007 was assessed by *Ye et al*. [2013]. *Zhang et al*. [2014] examined the impact of changes in the hydrological regime of Poyang Lake (in particular droughts) on water supplies, irrigation, and ecosystems for the last four decades. For the Xinjiang River basin of the Poyang Lake, *Guo et al*. [2008] examined the climate, land use, and land-cover effects on hydrology and streamflow using the SWAT model. They found that the climate effect is dominant in annual streamflow, while land-cover change influences seasonal streamflow and alters the annual hydrograph of the basin. *Wei et al*. [2015] investigated to which extent the tagged evaporated water from the Poyang Lake region returns to the land surface as precipitation.

3.2. Data

Driving Data. For the dynamical downscaling with the WRF-ARW model, the global reanalysis product ERA INTERIM [*Dee et al*., 2011] from the European Centre for Medium-Range Weather Forecasts (ECMWF) is chosen. The horizontal and temporal resolutions are T255 (approximately 0.75°) and 6 h, respectively.

In comparison to the standard WRF setup, the fully coupled modeling system requires additional static boundary information, characterizing the surface and subsurface conditions for the hydrological part. For the subsurface data, the Chinese Geology Dataset (1:400,000,000 scale) was used to derive hydrogeological input such as aquifer thickness, porosity, and saturated hydraulic conductivity. For the Poyang Lake basin, the aquifer thickness increases in general from the fringe areas toward the central part and Poyang Lake. Forty-three percent (93%) of the basin area have aquifer thicknesses of less than 100 m (500 m). Hydraulic conductivity is below 10^{-8} m/s in 17% of the basin area mainly in the mountainous region and increases toward Poyang Lake. In total, hydraulic conductivities below 10^{-6} m/s (10^{-5} m/s) occur in 73% (93%) of the basin area. Furthermore, the high-resolution digital elevation data set HYDRO1K from the U.S. Geological Survey with 1 km spatial resolution was used and upscaled to 10 km resolution to derive a consistent river network and its main characteristics, e.g., river depth, water surface elevation, and upstream area. For the

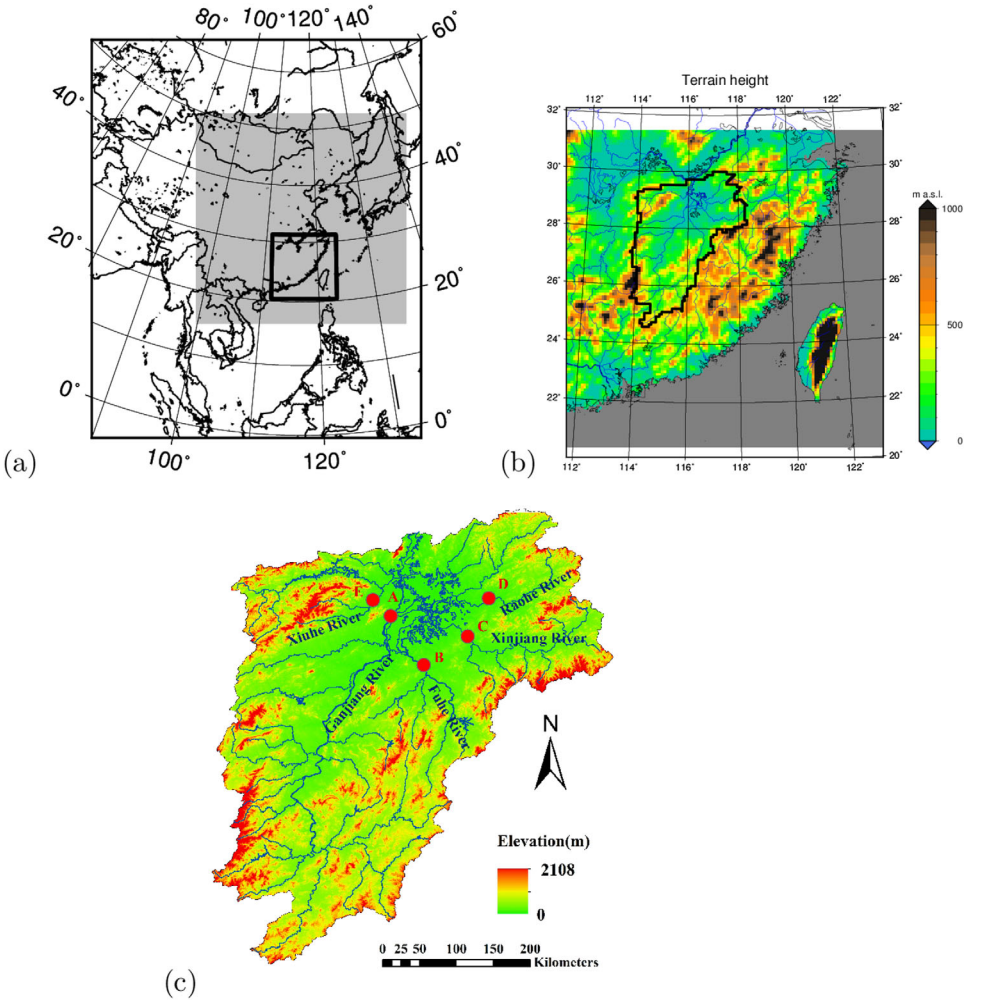

Figure 2. Maps of the simulation domains indicating (a) the coarse 30 km and fine 10 km nest and (b) the DEM of the 10 km nest; (c) river network and streamflux gauges of the Poyang Lake basin.

calculation of river depth, the product of the GIS-derived upstream area and an assumed local river input of 0.5 mm/d is used with an empirical channel width-to-depth relationship [see *Yu et al.*, 2006].

For the stand-alone HMS simulations, observed meteorological forcing data are required. The data sets encompass air temperature, air relative humidity, surface pressure, wind speed, surface downward longwave radiation, surface downward solar radiation, and precipitation. For this study, daily routine meteorological data for the years 1977–1986 from 26 meteorological stations were used. The station records were spatially interpolated onto the 10 km WRF grid using the bilinear interpolation method. Topographical effects were not considered for precipitation interpolation. However, for near-surface air temperature, a constant lapse rate of 0.65°C/100 m is applied to account for the differences between the elevation of the 10 km WRF grid cells and the stations. For the disaggregation of daily precipitation data to a 30 min time interval, an empirical equation based on the observed precipitation data statistics gathered at short time intervals was used [*Kondo and Xu*, 1997]. For the calculation, it is assumed that the distribution of the 30 min precipitation within a day follows a pattern of sinusoidal function and that the downscaled 30 min precipitation from the function is randomly distributed within the day for disaggregation.

Validation Data. For the validation of atmospheric variables, publicly available observational data sets for the time period 1979–1986 are applied. For temperature and precipitation, the Climate Research Unit (CRU) data set [*Mitchell and Jones*, 2005] is adopted which provides mean monthly surface data on a 0.5°

resolution. For precipitation, the data sets of the Global Precipitation Climatology Centre (GPCC) [*Schneider et al*., 2011] and the Asian Precipitation-Highly Resolved Observational Data Integration Towards Evaluation of Water Resources (APHRODITE) [*Yatagai et al*., 2012] are additionally used. GPCC contains globally monthly precipitation with a spatial resolution of 0.5°. The APHRODITE project provides a daily gridded precipitation data set across Asia in 0.25° resolution.

For the validation of the land surface variables for the given time period 1979–1986, the reanalysis product from the Climate Prediction Center (CPC) from NOAA [*Fan and van den Dool*, 2004] is used. It is a 0.5° monthly global product for soil moisture, evaporation, and runoff based on a one-layer hydrological model driven by observed precipitation and temperature. The depth of the soil column is 1.6 m assuming a fitted maximum holding capacity of 76 cm and a defined porosity of 0.47. For evapotranspiration, in addition, the *Global Land Evaporation: Amsterdam Methodology* (GLEAM) data set [*Miralles et al*., 2011] is used.

Daily streamflow data for 1978–1986 of the five downstream hydrological stations (Waizhou, Lijiadu, Meigang, Hushan, and Wanjiabu) of the main tributaries of Poyang Lake (Figure 2c and Table 3) are used for calibration and validation.

3.3. Simulation Design

The application of the fully coupled model system requires three steps: first, uncoupled simulations of the dynamical regional atmosphere model WRF-ARW to identify a suited setup for the target region (section 4.1). Second, for the setup and calibration of the hydrological model, stand-alone HMS simulations driven by meteorological observation data are performed and validated (section 4.2). Moreover, the impact of groundwater coupling on stand-alone HMS is elaborated (section 4.3). Third, the performance of fully coupled WRF-HMS simulations using the identified optimal stand-alone WRF and HMS setups is investigated (section 4.4).

HMS stand-alone simulations start in 1977 and the periods for model calibration and validation are 1978–1981 and 1982–1986, respectively, considering a full year for model spin-up. The fully coupled WRF-HMS simulations start in 1979 in accordance with the beginning year of the global forcing data ERA-Interim.

4. Results

In the following, the stand-alone WRF results are denoted as *R-WRF* (R: Results), stand-alone HMS results as *R-HMS* and stand-alone HMS with groundwater coupling results as *R-HMS-GW*. The results of the fully coupled atmospheric-hydrological model system are denoted as *R-WRF-HMS* without and as *R-WRF-HMS-GW* with groundwater coupling.

4.1. WRF Stand-Alone Setup for the Poyang Lake Region

For the Poyang Lake region, a two nest approach of WRF using Lambert conformal map projection is applied. The mother domain extends over East China (141 × 141 grid points) at a 30 km resolution. The finer nest covers the Poyang Lake basin and the near surroundings (124 × 124 grid points) at a 10 km resolution (see Figure 2a). A two nest approach with a coarse domain of 30 km was selected to allow simulations with coarser GCM driving data, e.g., other reanalysis products or global climate models for climate impact studies. The model uses 38 vertical levels for both nests. It is known that the performance of the stand-alone WRF simulations is sensitive to the selected WRF physics parametrizations, e.g., *Argüeso et al*. [2011], *Berg et al*. [2013], and *Fersch and Kunstmann* [2014]. Therefore, a number of WRF configurations covering several cumulus, microphysics, radiation, and planetary boundary layer parameterization schemes were investigated and validated for temperature and precipitation for the Poyang Lake basin [*Wagner et al*., 2013]. Based on these results and subsequent long-term sensitivity simulations, the following set of WRF model physics is selected: the WRF Single-Moment five-class scheme (WSM5) microphysical parameterization [*Hong et al*., 2004; *Hong and Lim*, 2006], the Betts-Miller-Janjić scheme [*Betts*, 1986; *Betts and Miller*, 1986; *Janjic*, 2000] for cumulus parameterization, the Yonsei University (YSU) parameterization [*Hong et al*., 2006] for the planetary boundary layer, the MM5-Dudhia shortwave scheme [*Dudhia*, 1989], and the Rapid Radiative Transfer Model (RRTM) longwave radiation scheme [*Mlawer et al*., 1997]. Due to our coupling approach, the Noah-LSM [*Chen and Dudhia*, 2001] was selected as land surface parameterization scheme.

In Figure 3a, the simulated monthly temperatures averaged over the Poyang Lake basin are shown. The CRU data set is added for comparison and statistical evaluation (see also Table 1). The comparison shows

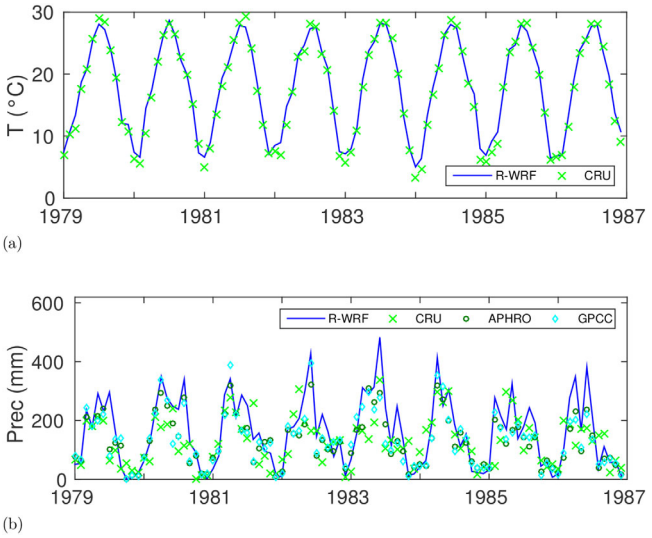

Figure 3. Spatially averaged (a) simulated (R-WRF) and observed (CRU) monthly temperature and (b) simulated (R-WRF) and observed (CRU, APHRODITE, and GPCC) monthly precipitation for the Poyang Lake basin.

that the selected WRF setup is able to simulate the observed annual cycle. Annual mean temperature is overestimated by 0.5°C and the correlation coefficient is R = 0.99. On seasonal scale, mean temperatures are mainly overestimated in winter and spring.

For precipitation, simulated monthly amounts averaged over the Poyang Lake basin are shown in Figure 3b. For validation, different observation data sets (see section 3.2) are added. The simulation results and performances are summarized in Table 2. In general, the stand-alone WRF simulation overestimates precipitation, in particular, during the rain intensive months in spring and summer. On annual scale, WRF overestimates precipitation by 21–26% depending on the validation data set. Figure 3b and Table 2 also depict a distinct variability within the different validation sets. Annual precipitation amounts are comparable, but the correlation coefficient implies differences. The correlation between GPCC and APHRO is high (R = 0.97) whereas the correlation coefficient between CRU and one of the other two data sets is R = 0.64. The correlation coefficients between WRF and the validation data sets of APHRO (R = 0.90) and GPCC (R = 0.87) are also higher compared to the CRU data set (R = 0.68).

4.2. HMS Stand-Alone Setup for the Poyang Lake Region

The HMS simulations use the same grid as the innermost domain of the WRF setup. In hydrological modeling, the initial groundwater level and soil moisture conditions play a central role for simulating the terrestrial water balance. To account for this, spin-up simulations are performed until the system reaches or approximates equilibrium conditions. For the HMS simulations, the state variables of the last time step of the spin up simulation are then used as initial conditions. The calibration of the Noah-LSM and HMS parameters was performed manually. Simulation results were evaluated visually (e.g., annual cycles) and by comparison of efficiency criteria like mean bias, coefficient of determination (R), and Nash-Sutcliffe Efficiency (NSE). Therefore, several sensitivity runs starting from literature or default values and using the physically feasible range for each calibration parameter and different combinations were performed. The evaluation has shown that for the Noah-LSM, the surface runoff parameter *REFKDT* and the bare soil evaporation exponent *FXEXP* are the most sensitive parameters in this study. For the HMS model, it is the Manning's roughness coefficient and the streambed conductivity, which controls the interaction between water in the river and the unsaturated or saturated zone. The final parameter values are 3.0 for *REFKDT*, 1.0 for *FXEXP*, a Manning's roughness coefficient of 0.02 ($s/m^{1/3}$), and 10^{-5} (1/s) for streambed conductivity.

In Figure 4, streamflow estimations of the stand-alone HMS simulations (R-HMS) at the downstream gauges of the five main tributaries of Poyang Lake are depicted. The simulated streamflows are in reasonable agreement with the observations. HMS is capable to simulate the observed intra-annual and inter-annual variabilities. However, for three catchments (Ganjiang-Waizhou, Xinjiang-Meigang, and Xiuhe-Wanjiabu), base flow is underestimated. For Meigang, HMS also underestimates peak flows. The scatterplot in Figure 4f indicates the large range of streamflow observations and simulation results. There is no overall tendency of underestimation or overestimation. In Table 3, the performances of the streamflow estimates of the

Table 1. (top) Seasonal and Annual Mean Temperature (°C) of Stand-Alone WRF (R-WRF) and CRU and (bottom) Performance Statistics for the Poyang Lake Region for 1979–1986

	DJF	MAM	JJA	SON	ANNUAL
R-WRF	7.8	18.0	26.9	19.1	18.0
CRU	7.0	16.9	27.3	19.0	17.5

	BIAS (°C)	RMSE (°C)	R
R-WRF versus CRU	0.5	1.1	0.99

Table 2. (top) Seasonal (mm/month) and Annual Precipitation (mm/year) of Stand-Alone WRF (R-WRF) and APHRO, CRU, or GPCC and (bottom) Performance Statistics for the Poyang Lake Region for 1979–1986

	DJF	MAM	JJA	SON	ANNUAL
R-WRF	61	266	234	88	1948
APHRO	68	212	163	78	1564
CRU	68	210	160	77	1547
GPCC	73	224	160	79	1606

	BIAS (mm/month)	RMSE (mm/month)	R
R-WRF versus APHRO	32	64	0.90
R-WRF versus CRU	33	92	0.68
R-WRF versus GPCC	29	66	0.87

stand-alone HMS simulations are evaluated. For the main tributary, the Ganjiang River with the gauge Waizhou, the best overall performance is achieved with NSE values of 0.75 (calibration) and 0.71 (validation) on daily scale and 0.89 for both time periods on monthly scale. For the other four basins, NSE values are within the range of 0.33 and 0.72 (calibration) and 0.44 and 0.68 (validation) for daily values, and 0.56–0.88 (calibration) and 0.72–0.86 (validation) on monthly scale. The mean bias ranges from −19 to +27% (−15 to +19%) for the calibration (validation) period. The performance differences between the catchments may also be attributed to uncertainties in the meteorological forcing and the effects of human activities in the watershed, because HMS can only generate natural flow conditions. The performances are comparable for both, calibration and validation periods. In general, the correlation coefficient as well as NSE values indicate a performance increase with larger catchment size.

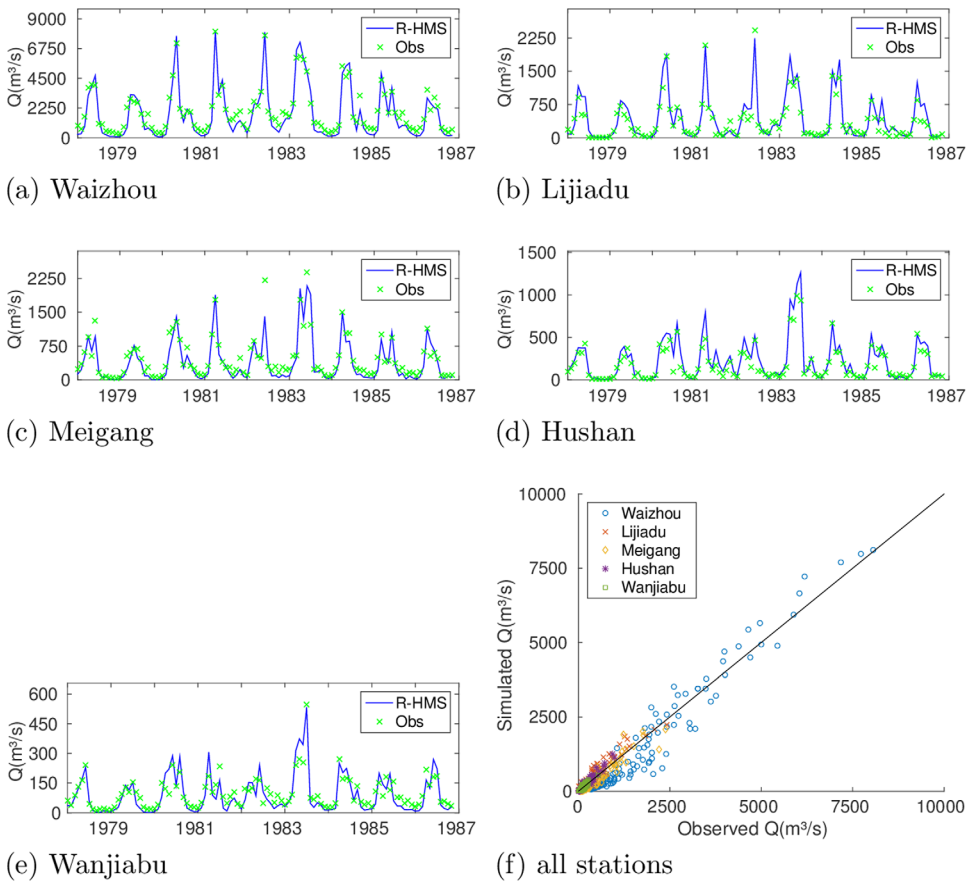

Figure 4. (a–e) Simulated (blue) and observed (green) monthly streamflow for the tributaries of Poyang Lake using the standalone HMS setup; (f) scatterplot of simulated and observed streamflows at all five gauges.

Table 3. (top) List of gauging stations and (bottom) Performance of Stand-Alone HMS Simulations for the Main Tributaries of Poyang Lake for the Calibration (1978–1981) and Validation Period (1982–1986)

Index	Station	River	Catchment Size (km^2)
A	Waizhou	Ganjiang	80,948
B	Lijiadu	Fuhe	15,811
C	Meigang	Xinjiang	15,535
D	Hushan	Raohe	6,374
E	Wanjiabu	Xiuhe	3,548

Station		Qobs (m^3/s)	Qsim (m^3/s)	BIAS (%)	R	NSE (Daily)	NSE (Monthly)
Waizhou	Cal	1,907	1,626	−15	0.88	0.75	0.89
	Val	2,141	1,886	−12	0.87	0.71	0.89
Lijiadu	Cal	357	388	9	0.85	0.72	0.87
	Val	376	446	19	0.85	0.68	0.83
Meigang	Cal	434	349	−19	0.80	0.62	0.88
	Val	497	421	−15	0.81	0.65	0.86
Hushan	Cal	160	203	27	0.76	0.53	0.66
	Val	205	238	16	0.82	0.66	0.86
Wanjiabu	Cal	86	77	−10	0.58	0.33	0.56
	Val	108	99	−8	0.67	0.44	0.72

4.3. HMS Simulations With Groundwater Feedback

As described in section 2.4, two different approaches, the *Fixed-head* boundary and *Darcy-flux* approximation, were implemented for describing the coupling between groundwater and LSM. For the analysis, simulation results with embedded groundwater feedback are compared with the stand-alone HMS results of section 4.2. The two-way coupling primarily impacts the flux at the lower boundary of the LSM, which is denoted as recharge in the following. Downward fluxes have positive signs and upward fluxes negative signs.

For the analysis of the impact of groundwater feedback, simulation results using the *Fixed-head* lower boundary condition (R-HMS-GW) are compared with the uncoupled simulations (R-HMS) first. Second, the impact of the *Darcy-flux* coupling method is investigated.

Fixed-Head Coupling Method. The time series of the spatially averaged recharge amounts of R-HMS and R-HMS-GW indicate similar annual cycles and long-term simulation results (see Figure 5, top). The difference plot (Figure 5, bottom) indicates higher spatially averaged monthly recharge amounts with groundwater coupling, even though the implementation of groundwater feedback methods would also allow for upward (negative) fluxes. Furthermore, the differences show a clear annual cycle with largest differences between March and July, approximately following the course of the absolute recharge amounts. This means that the parameterization of recharge as flux at the bottom boundary in the Noah-LSM results in general to lower recharge rates in comparison to the approach allowing bidirectional groundwater feedback. As described in section 2.1, subsurface runoff amounts in standard Noah-LSM depend on the hydraulic conductivity and the slope coefficient value. As a sensitivity test, a simulation with the maximum feasible value of 1.0 for the slope coefficient was performed in addition to the simulation with the default value of 0.1. The simulation with the value of 1.0 results in increased subsurface runoff. The spatially averaged total amounts are still lower in comparison to the approach

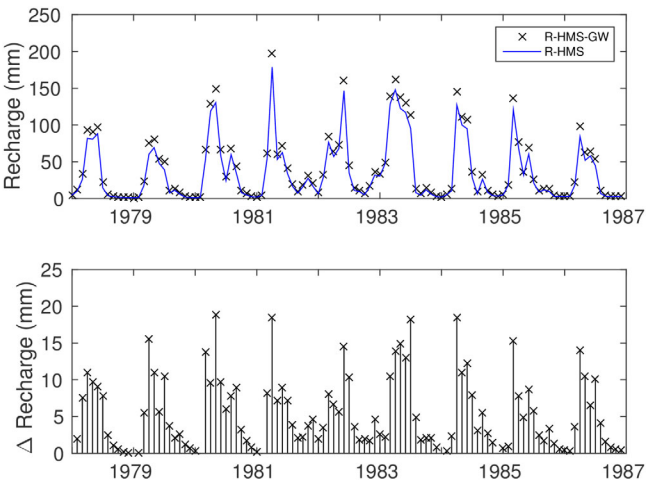

Figure 5. (top) Spatially averaged simulated monthly recharge amounts and (bottom) the respective differences without (R-HMS) and with (R-HMS-GW) groundwater coupling (Fixed-head boundary method) for the Poyang Lake basin.

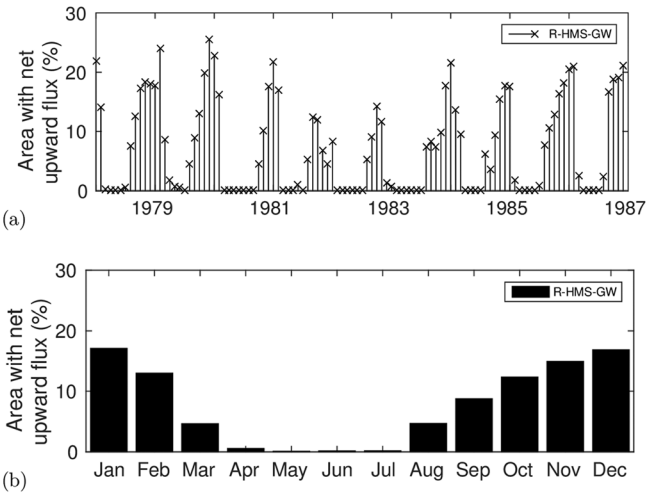

Figure 6. (a) Time series of the area (%) with net upward recharge amounts and (b) corresponding mean annual cycle of the R-HMS-GW simulation with groundwater coupling (Fixed-head boundary method) for the Poyang Lake basin.

allowing bidirectional groundwater feedback (not shown).

Although the spatially averaged recharge amounts with groundwater coupling are higher than those without coupling, upward fluxes occur in the Poyang Lake basin, in particular around the Poyang Lake in the northern part of the basin. In Figure 6a, the monthly time series of the percentage of the basin area with net upward fluxes is depicted. It shows that the percentage of the basin with dominant upward fluxes varies between almost 0% and 27%. There is a distinct annual cycle in this time series with minimum values from approximately April to July and maximum values in December and January (see Figure 6b). The comparison with Figure 5a indicates that net upward fluxes mainly occur during time periods of small absolute recharge amounts. And in comparison to the annual cycle of precipitation, the percentage area of net upward fluxes is maximal in the months after the rainy season.

As consequence of the impact of the two-way coupling between groundwater and LSM on recharge rates, further variables of the terrestrial water cycle are affected. Changes in the bottom drainage of the LSM first impact soil moisture in the lowest soil layer of the LSM, which in turn alters the conditions in the overlying layers up to the land surface. In Figure 7, the time series of the spatially averaged soil moisture conditions of R-HMS and R-HMS-GW are shown for the near-surface (top) and deep soil layer (bottom). For the deep soil layer, the impact of implementing groundwater feedback methods is clearly visible. Due to higher recharge amounts with groundwater coupling, the deep soil is drier compared to the uncoupled results. On average, the volumetric soil moisture is reduced by 0.037 (−10%). For the top soil layer, the differences between R-HMS and R-HMS-GW are smaller, but in accordance to the deep soil layer, the results with feedback indicate drier soil moisture conditions. On average, the volumetric soil moisture in the top soil layer is reduced by 0.014 (−4%).

These changes in soil moisture in the top soil layer impact the processes at the land surface. This is demonstrated in Figure 8, which shows the time series of the spatially averaged evapotranspiration and surface runoff for R-HMS and R-HMS-GW. In general, the annual cycles and long-term simulation results of the coupled and uncoupled simulations are similar for both variables. Only minor differences occur. The implementation of groundwater feedback results in slightly lower evapotranspiration and surface runoff amounts. On annual scale, a reduction of 21 mm (−3%) for evapotranspiration and 43 mm (−15%) for surface runoff was simulated.

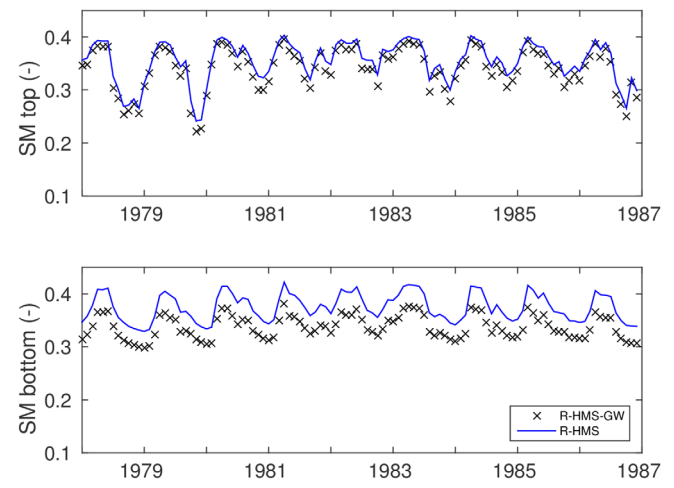

Figure 7. Spatially averaged simulated monthly mean soil moisture of (top) near-surface soil layer and (bottom) deep soil layer without (R-HMS) and with (R-HMS-GW) groundwater coupling (Fixed-head boundary method) for the Poyang Lake basin.

Darcy-Flux Coupling Method. The analysis of the simulation results with the *Darcy-flux* coupling method reveals a very similar impact of implementing groundwater

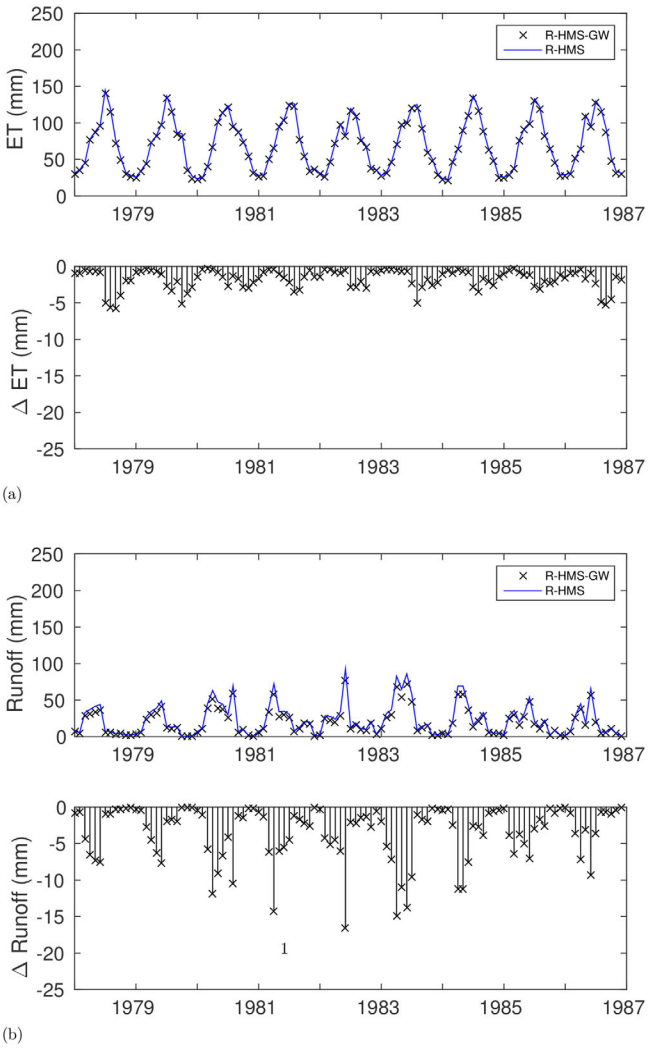

Figure 8. (a) Spatially averaged simulated monthly evapotranspiration and (b) surface runoff amounts and the respective differences without (R-HMS) and with (R-HMS-GW) groundwater coupling (Fixed-head boundary method) for the Poyang Lake basin.

feedback as the results of the *Fixed-head* approach. For the variable recharge, which is primarily impacted by the coupling, monthly differences are in the range of ±0.6 mm. In total, the recharge amount using the *Fixed-head* boundary condition is 2.3 mm (0.05%) higher. Due to the minor differences between the simulation results of the two coupling methods for recharge, the results for other variables of the terrestrial water cycle are also very similar (not shown). These findings are in accordance with the results of a one-dimensional sensitivity study for the TERENO preAlpine observatory in Southern Germany [*Fersch et al.*, 2013].

4.4. Fully Coupled WRF-HMS Simulations

For the fully coupled atmospheric-hydrological simulations, the identified stand-alone setups of WRF (see section 4.1) and HMS (see section 4.2) for the Poyang Lake region were used. The fully two-way coupled model system enables, in addition to the investigations of the impact of groundwater coupling on land surface variables (see section 4.3), also the feedback analysis for atmospheric variables, in particular temperature and precipitation. For this purpose, the model system is applied in two configurations: one simulation without groundwater feedback (R-WRF-HMS) and one simulation which additionally considers bidirectional water fluxes between groundwater and LSM (R-WRF-HMS-GW). Due to the high computational demand of high-resolution standard WRF and the fully coupled simulations and the fact that the simulation results for both coupling methods have been demonstrated to be very similar (see section 4.3), we

Table 4. Performance of Fully Coupled WRF-HMS Simulations Without and With Groundwater Coupling for the Main Tributaries of Poyang Lake for the Time period 1979–1986

Station	Qobs (m^3/s)	Qsim (m^3/s)	BIAS (%)	R	NSE (Daily)	NSE (Monthly)
Without Groundwater Coupling						
Waizhou	2096	2102	~0	0.77	0.33	0.48
Lijiadu	385	501	30	0.72	0.23	0.39
Meigang	482	509	6	0.66	0.14	0.42
Hushan	192	270	41	0.59	−0.51	−0.04
Wanjiabu	102	117	15	0.58	−0.02	−0.14
With Groundwater Coupling						
Waizhou	2096	2090	~0	0.78	0.38	0.58
Lijiadu	385	471	22	0.70	0.20	0.49
Meigang	482	489	~0	0.63	0.17	0.48
Hushan	192	268	40	0.55	−0.61	0.02
Wanjiabu	102	118	16	0.56	−0.10	−0.13

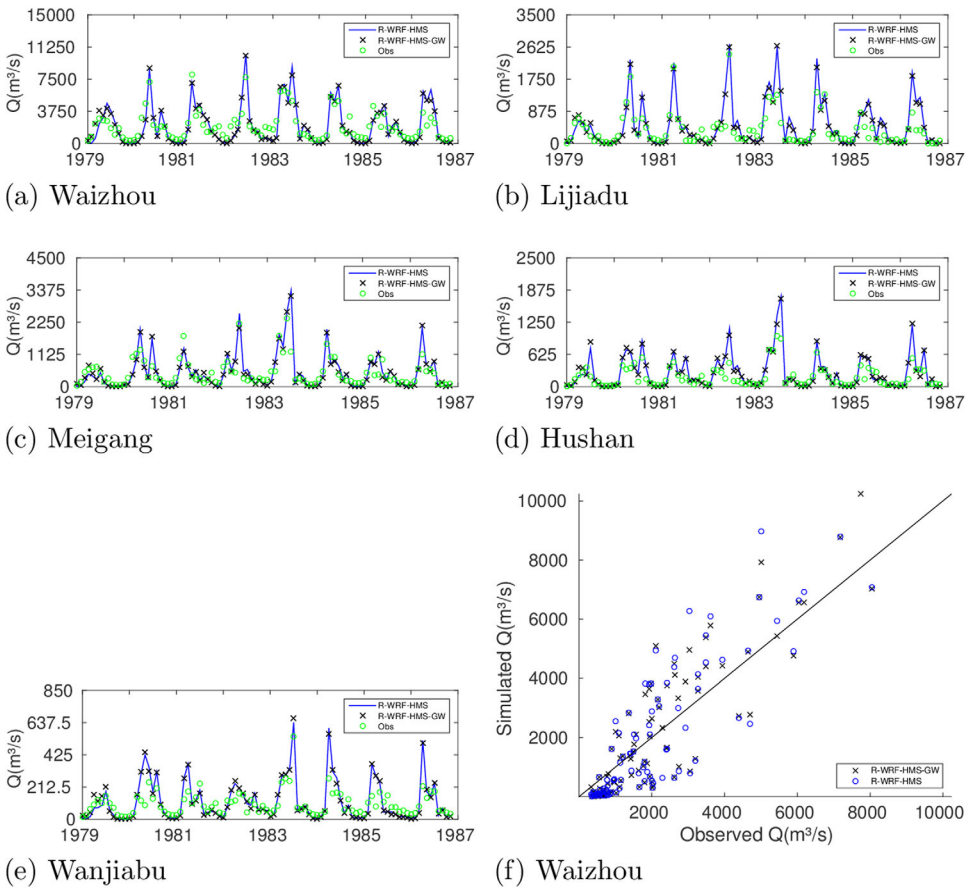

Figure 9. Simulated and Observed (green) monthly streamflows of the tributaries of Poyang Lake using the fully coupled WRF-HMS setup without (blue) and with (black) groundwater coupling.

performed one fully coupled model run with enabled groundwater feedback. We selected the *Fixed-head* method, because it is mass and energy conservative and contains less parameterizations than the *Darcy-flux* method.

The simulation period 1979–1986 allows a multiyear analysis of the feedback mechanisms and quantities, which is presented in the following and summarized in Tables 4 and 5.

Streamflow. According to the stand-alone HMS analysis, streamflow estimations of the fully coupled model system are investigated at the downstream stations of the five main tributaries of Poyang Lake (Figure 9). In general, the fully coupled model system is able to simulate streamflow reasonable in terms of seasonal cycle and long-term, inter-annual variability. Furthermore, the impact of groundwater feedback on predicted streamflow is minor. This is because runoff generation is dominated by surface runoff and the groundwater table is relatively deep with an average depth of 40 m in this study. For that reason, the contribution of the channel-groundwater flow interaction on streamflow is minor, which might also cause the underestimations in simulated base flow. The scatterplot for the gauge Waizhou in Figure 9f also illustrates the underestimation of base flow and comparable performances of the simulations with and without groundwater feedback. Altogether, the performance of both fully coupled simulation results is lower in comparison to the stand-alone R-HMS results in Figure 4. The performance differences between the stand-alone and fully coupled simulations can be mainly explained by deviations in the meteorological forcing. In the stand-alone simulations, HMS is driven by observed meteorology, whereas in the fully coupled version, the biases of the WRF simulations propagate into the hydrological part. The validation of the stand-alone WRF simulations depicted an overestimation for precipitation in the rain intensive months, in particular, for the years 1983 and 1986 (see Figure 3b). For these 2 years, the fully coupled WRF-HMS model system also simulates highest overestimations of peak flow for all gauges. Furthermore, the

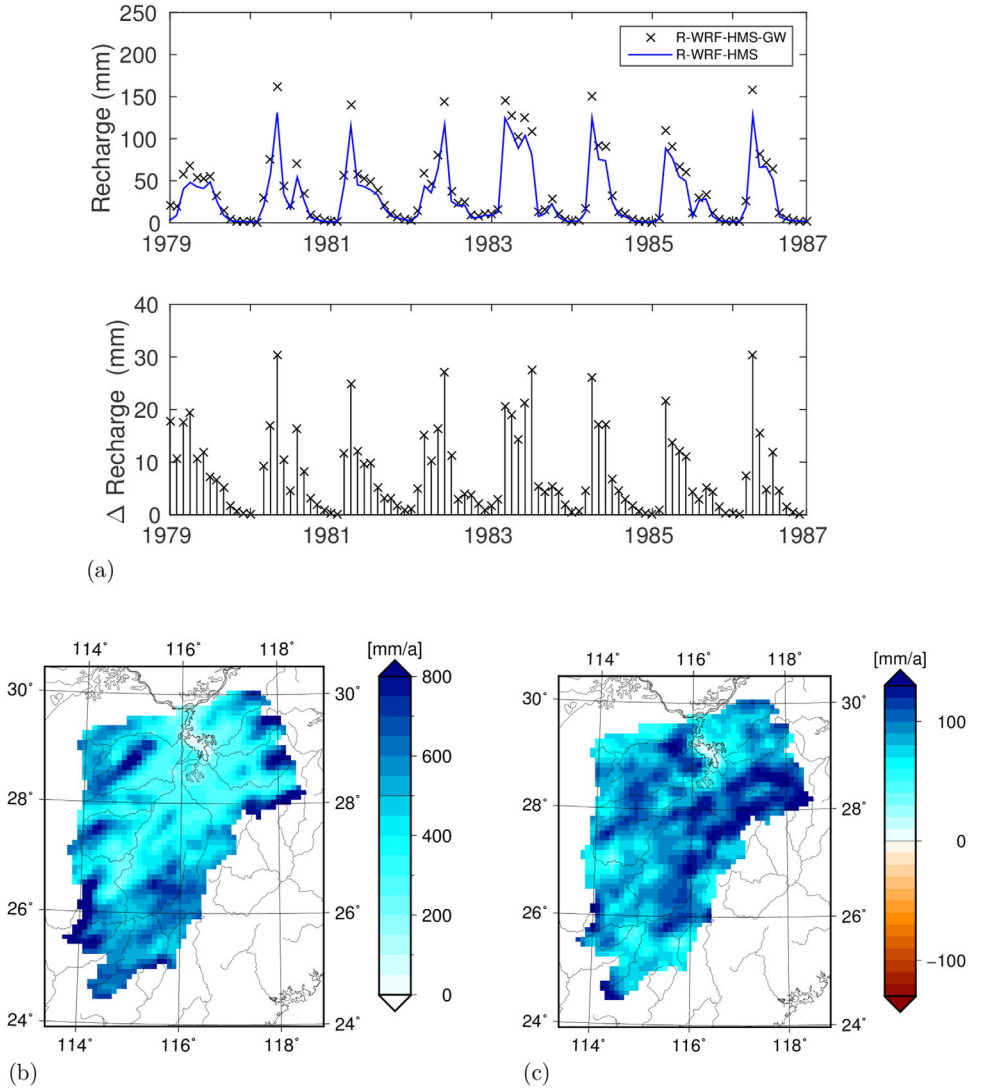

Figure 10. (a) Spatially averaged simulated monthly (top) recharge amounts and (bottom) differences of the fully coupled simulations R-WRF-HMS (blue) and R-WRF-HMS-GW (black); (b) spatial distribution of mean annual recharge (mm) of R-WRF-HMS-GW and (c) corresponding mean annual differences (mm) compared to R-WRF-HMS for the Poyang Lake basin.

underestimation of precipitation in 1981 results in underestimations in streamflow in two large subcatchments at the gauges Waizhou and Meigang. These findings corroborate the significant impact of atmospheric simulation quality, in particular precipitation, on the performance of the fully coupled modeling system with respect to hydrology.

In Table 4, the performance of the streamflow estimations of the fully coupled WRF-HMS simulations is summarized. For R-WRF-HMS, NSE values for the main tributary, the Ganjiang basin with the gauge Waizhou, are 0.33 on daily and 0.48 on monthly scales. For the other four basins, NSE values are within the range of −0.52 and 0.23 for daily and between −0.14 and 0.42 for monthly values. The mean bias is up to +41% mainly due to the overestimations in simulating peak flow. The low NSE values and the maximum bias occur in the two smallest subcatchments. In particular, in smaller catchments, uncertainties and spatial shifts in the precipitation patterns may result in poorer performances of streamflow. The comparison of the performance of fully coupled simulations with and without groundwater feedback shows some minor differences. On daily scale, there is no clear tendency of improvement, but on monthly scale, NSE values of the simulations with groundwater feedback are increased by up to 0.1 for the gauges Waizhou and Lijiadu.

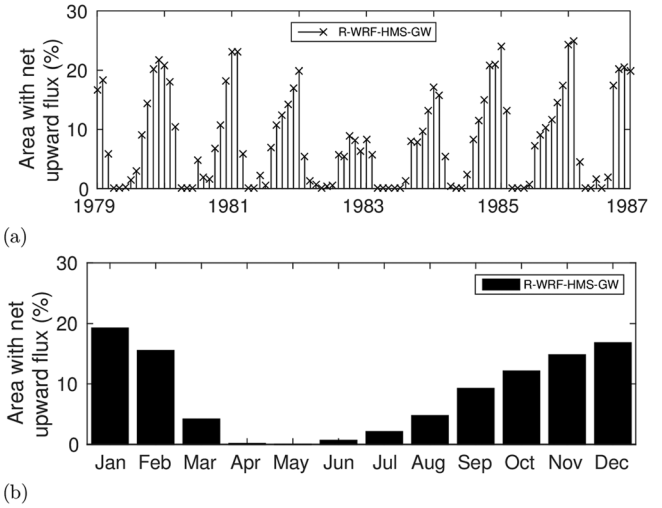

Figure 11. (a) Time series of the area (%) with net upward recharge amounts and (b) corresponding mean annual cycle of the fully coupled simulations R-WRF-HMS-GW for the Poyang Lake basin.

Recharge. Figure 10a compares the spatially averaged recharge rates for R-WRF-HMS and R-WRF-HMS-GW. The recharge time series of both simulations depict comparable annual cycles and long-term results. The time series of differences indicate in particular higher monthly recharge amounts with groundwater coupling between March and July. The results are in line with the findings for the stand-alone HMS simulations in Figure 5. However, for the fully coupled model system, the differences, whether using groundwater coupling or not are larger compared to the stand-alone simulations. This is mainly due to the general tendency of overestimation for precipitation as discussed in section 4.1.

In accordance to the findings for stand-alone HMS, also upward fluxes occur in the Poyang Lake basin (see Figure 11). The percentage of the basin area with net upward fluxes varies between almost 0% and 25%. The annual cycle indicates a slightly higher percentage of the basin area with dominant upward fluxes in comparison to the stand-alone HMS results. Therefore, the annual mean percentage of the area with net upward flux is 8.3% for the fully coupled simulations, while it is 7.5% for the stand alone ones.

Figure 10b shows the spatial distribution of annual recharge of the R-WRF-HMS-GW simulation. Distinct recharge areas are located along the boundaries and in the mountainous parts of the Poyang Lake basin. The spatial distribution of the differences between R-WRF-HMS-GW and R-WRF-HMS are shown in Figure 10c. According to the time series, positive differences indicate higher values with groundwater coupling. In general, annual recharge amounts with groundwater coupling increase on average by 95 mm (26%) for the Poyang Lake basin. The relative differences are larger around the Poyang Lake and for the flat regions where lower absolute recharge amounts were simulated (not shown). This means that for these regions there is a higher interaction between groundwater and LSM.

*Soil Moisture***.** Figure 12a shows the time series of spatially averaged soil moisture contents for R-WRF-HMS and R-WRF-HMS-GW. According to the stand-alone HMS results of Figure 7, the implementation of groundwater feedback results in drier conditions in the deep soil layer due to higher recharge amounts as discussed above. In comparison to R-WRF-HMS, the volumetric soil moisture of R-WRF-HMS-GW is reduced by 9.5% (3.5%) in the deep (top) soil layer.

Figure 12b shows the spatial distribution of mean annual soil moisture for the deep soil layer of R-WRF-HMS-GW for the Poyang Lake basin. The dark blue pixels represent the lake area and near surrounding with soil moisture contents up to saturation. In the basin, there is an increase of soil moisture from the upstream regions in the fringe area and southern part northward to the river valleys and the Poyang Lake. The results for the overlying soil layers are comparable (not shown). The spatially distributed differences of mean soil

Table 5. Impact of Fully Coupled WRF-HMS Simulations (R-WRF-HMS-GW) in Comparison to R-WRF-HMS on Surface Runoff, Recharge, Soil Moisture in the Top and Bottom Layer of the LSM, Evapotranspiration, 2 m Temperature, and Precipitation of the Poyang Lake Basin for the Period 1979–1986

	Runoff (mm)	Recharge (mm)	SM Top	SM Bottom	ET (mm)	T (°C)	P (mm)
R-WRF-HMS	442	371	0.315	0.364	1141	18.0	1942
R-WRF-HMS-GW	381	467	0.304	0.330	1112	18.1	1941
Absolute Differences	−61	95	−0.01	−0.03	−29	0.1	−1
Relative Differences	−14%	26%	−3.5%	−9.5%	−3%	0.5%	−0.03%

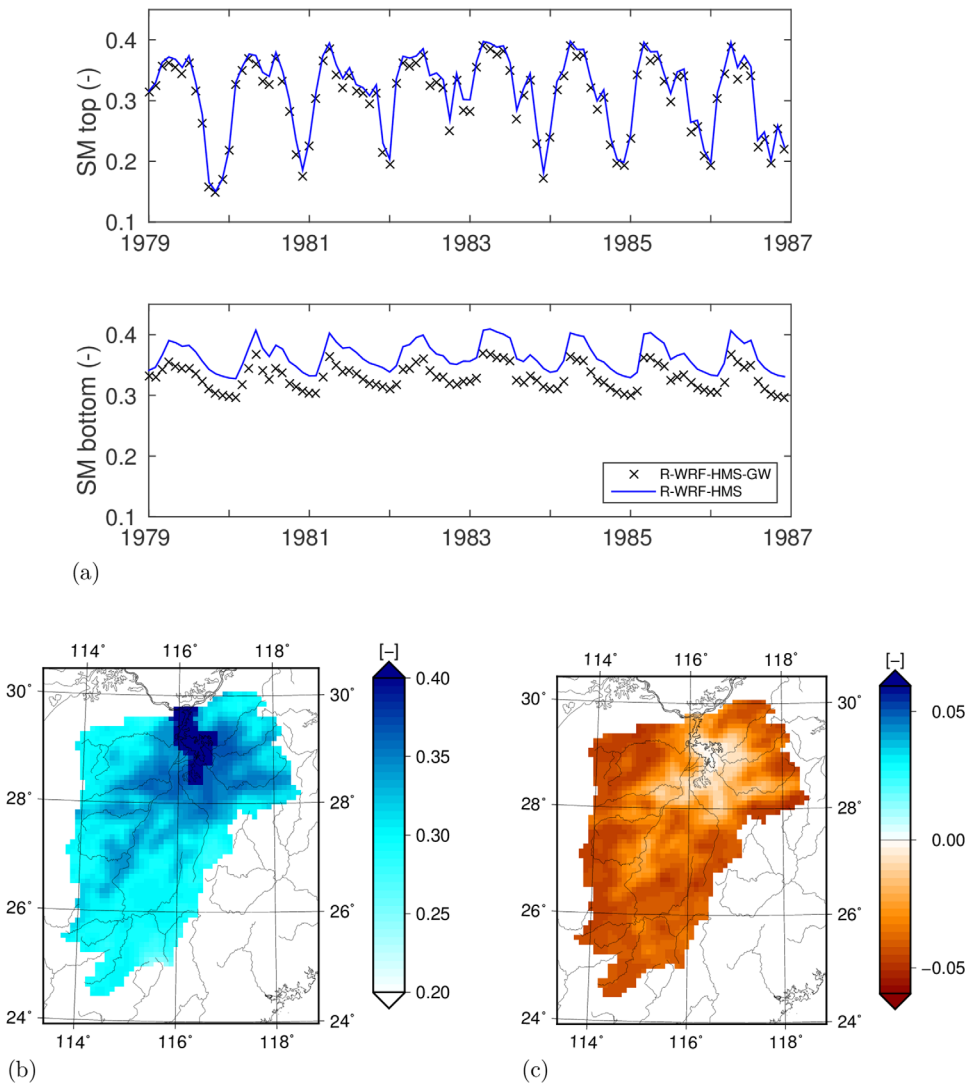

Figure 12. (a) Spatially averaged simulated monthly soil moisture of (top) near-surface soil layer and (bottom) deep soil layer of the fully coupled simulations R-WRF-HMS (blue) and R-WRF-HMS-GW (black); (b) spatial distribution of mean annual soil moisture of R-WRF-HMS-GW and (c) corresponding mean annual differences of the deep soil layer compared to results without groundwater coupling for the Poyang Lake basin.

moisture in the deep soil layer indicate basin-wide drier soil moisture conditions for R-WRF-HMS-GW (see Figure 12c). Around Poyang Lake and in the river valleys, the decrease in soil moisture is minor compared to the fringe areas of the basin. This tendency holds true also for the other overlying soil layers but witch decreasing magnitude (not shown).

Evapotranspiration. In Figure 13, the impact of altered soil moisture conditions on evapotranspiration is shown. The annual cycles of R-WRF-HMS and R-WRF-HMS-GW are in general comparable. However, the corresponding difference plot indicates an evapotranspiration decrease in the R-WRF-HMS-GW simulation with a mean annual difference of −29 mm (−3%). The spatial distribution of mean annual evapotranspiration of R-WRF-HMS-GW in Figure 13b shows beside the maximum values over the Poyang Lake, higher evapotranspiration rates in the eastern and southern part of the basin following mainly the spatial distribution of precipitation (see below). The corresponding spatial distribution of the mean annual differences shows, except for the Poyang Lake itself, a decrease in evapotranspiration using R-WRF-HMS-GW. The evapotranspiration increase for the Poyang Lake itself is connected to the increase in surface temperature in the fully coupled simulations (see below).

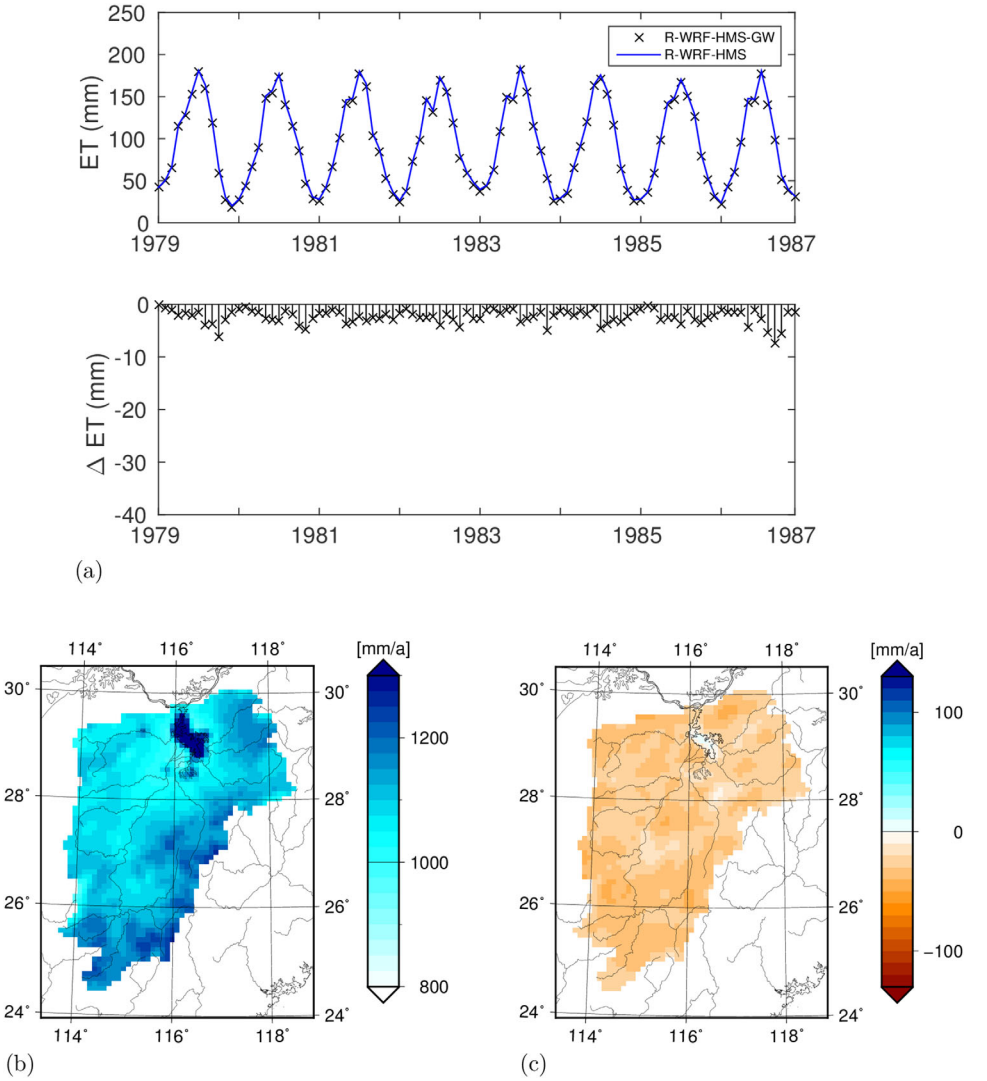

Figure 13. (a) Spatially averaged simulated monthly (top) evapotranspiration and (bottom) differences of the fully coupled simulations R-WRF-HMS (blue) and R-WRF-HMS-GW (black); (b) spatial distribution of mean annual evapotranspiration (mm) of R-WRF-HMS-GW and (c) corresponding mean annual differences (mm) compared to R-WRF-HMS for the Poyang Lake basin.

Surface Runoff. For surface runoff, the spatially averaged time series of both fully coupled simulations are comparable (Figure 14a). However, the corresponding time series of differences indicates a decrease in particular of the peaks in surface runoff with groundwater coupling. This decrease in surface runoff is mainly due to the increase in recharge in the fully coupled simulations with groundwater coupling (see Figure 10). On annual scale, surface runoff is reduced by 61 mm (−14%).

The spatial distribution of annual surface runoff indicates higher values in the northeastern part of the basin around the Poyang Lake (see Figure 14b). The corresponding difference plot (see Figure 14c) depicts in general a decrease of surface runoff in the Poyang Lake basin in particular in the fringe area using R-WRF-HMS-GW.

Temperature. In the fully coupled simulations, the altered soil moisture conditions at the land surface also impact the exchange with the atmospheric boundary layer and as a consequence atmospheric variables. This is investigated for temperature (Figure 15) and precipitation (Figure 16) below. The time series of spatially averaged temperatures of both simulations show similar annual cycles and long-term behavior. However, the difference plot depicts a clear signal of higher temperatures up to 0.2°C on monthly scale with groundwater coupling. In consequence, annual mean temperature increases from 18.0°C

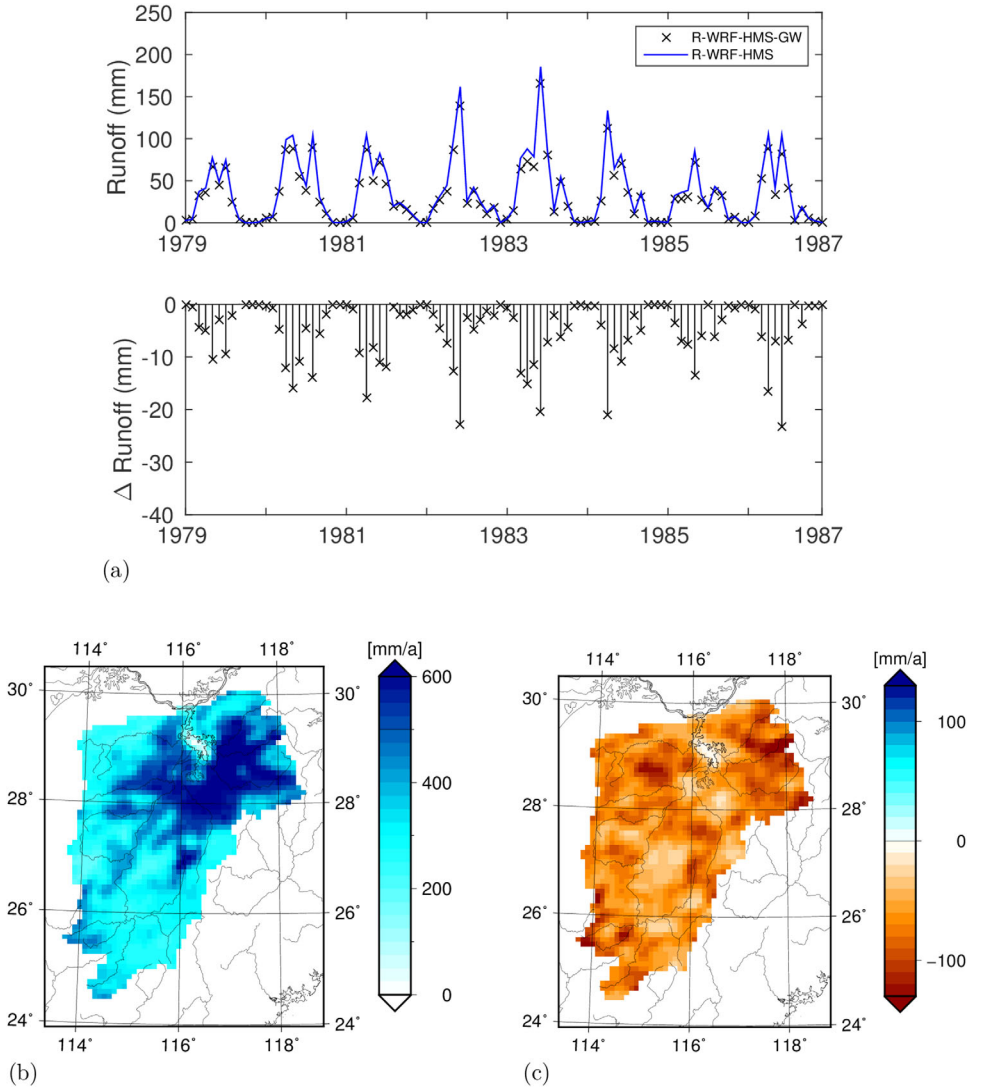

Figure 14. (a) Spatially averaged simulated monthly (top) surface runoff and (bottom) differences of the fully coupled simulations R-WRF-HMS (blue) and R-WRF-HMS-GW (black); (b) spatial distribution of mean annual surface runoff (mm) of R-WRF-HMS-GW and (c) corresponding mean annual differences (mm) compared to R-WRF-HMS for the Poyang Lake basin.

(R-WRF-HMS) to 18.1°C (R-WRF-HMS-GW). The spatial distribution of mean annual temperature shows a general increase from North to South and a distinct temperature gradient with height (see Figure 15b). The corresponding differences in mean annual temperature in Figure 15c indicate a basin wide temperature increase. The spatial pattern shows that the temperature increase is higher along the river valleys. The basin-wide increase in temperature and the decrease in evapotranspiration using groundwater coupling (discussed above) indicates a slight shift on the partitioning of surface turbulent fluxes toward higher sensible heat flux.

Precipitation. For precipitation (Figure 16), the time series of spatially averaged results of R-WRF-HMS and R-WRF-HMS-GW are, in accordance to the previous results, similar. However, the corresponding time series of differences exhibits no distinct impact, but changes with alternating signs in the range of $\pm$10 mm on monthly scale. The impact on mean annual precipitation amounts is minor with values of 1942 mm for R-WRF-HMS and 1941 mm for R-WRF-HMS-GW. Due to the fact that the initial conditions and the inflow of moisture at the domain boundaries is the same for both simulations, the spatial redistribution within the domain can be attributed to the groundwater feedback. For the Poyang Lake basin, this results in temporal shifts in the precipitation time series between the fully coupled simulations with and without groundwater

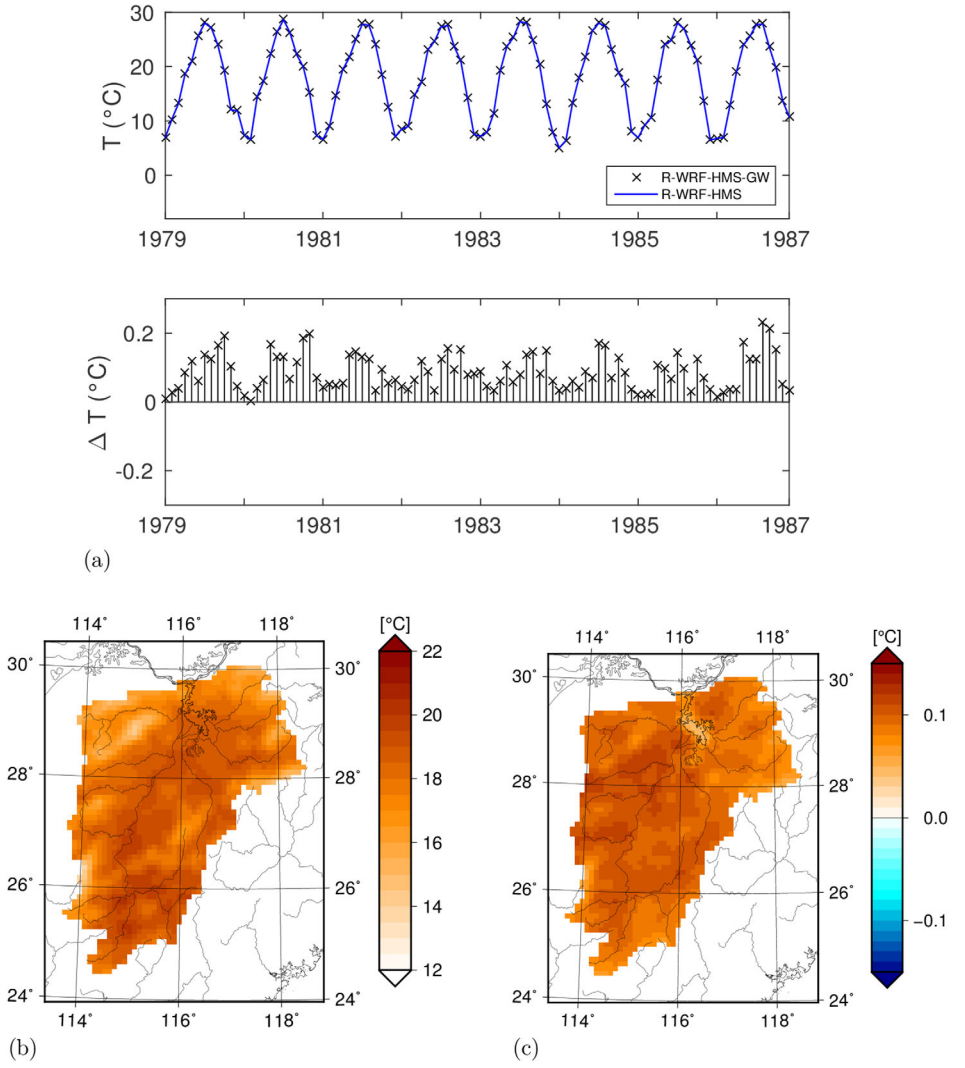

Figure 15. (a) Spatially averaged simulated monthly 2 m (top) temperature and (bottom) differences of the fully coupled simulations R-WRF-HMS (blue) and R-WRF-HMS-GW (black); (b) spatial distribution of mean annual 2 m temperature (°C) of R-WRF-HMS-GW and (c) corresponding mean annual differences (°C) compared to R-WRF-HMS for the Poyang Lake basin.

feedback, which balance on longer time scales. Within the Poyang Lake basin, annual precipitation amounts are higher in the North-East and South-West, whereas around the Poyang Lake and in the center of the basin lower precipitation amounts are simulated (see Figure 16b). The spatially distributed differences between R-WRF-HMS-GW and R-WRF-HMS indicate regional changes up to ±100 mm (±5%). It shows that there is no general tendency of higher or lower precipitation amounts using R-WRF-HMS-GW. Hence, in addition to the temporal shifts, there is a spatial redistribution within the domain which balances to a relatively small overall change on the Poyang Lake basin scale.

4.5. Evaluation of Fully Coupled WRF-HMS Simulations

In addition to the streamflow validation in section 4.4, results of the fully coupled WRF-HMS simulations are evaluated further. For the given time period 1979–1986, the Climate Prediction Center (CPC) of NOAA is used for the evaluation of evapotranspiration, runoff, and soil moisture. Therefore, time series of basin averaged evapotranspiration, runoff, and soil moisture are shown for the CPC product and the two fully coupled WRF-HMS simulations in Figure 17.

Evapotranspiration is overestimated by both simulations, which can be mainly attributed to the overestimation in precipitation occurring in spring and in particular in summer with values up to 75 mm per month

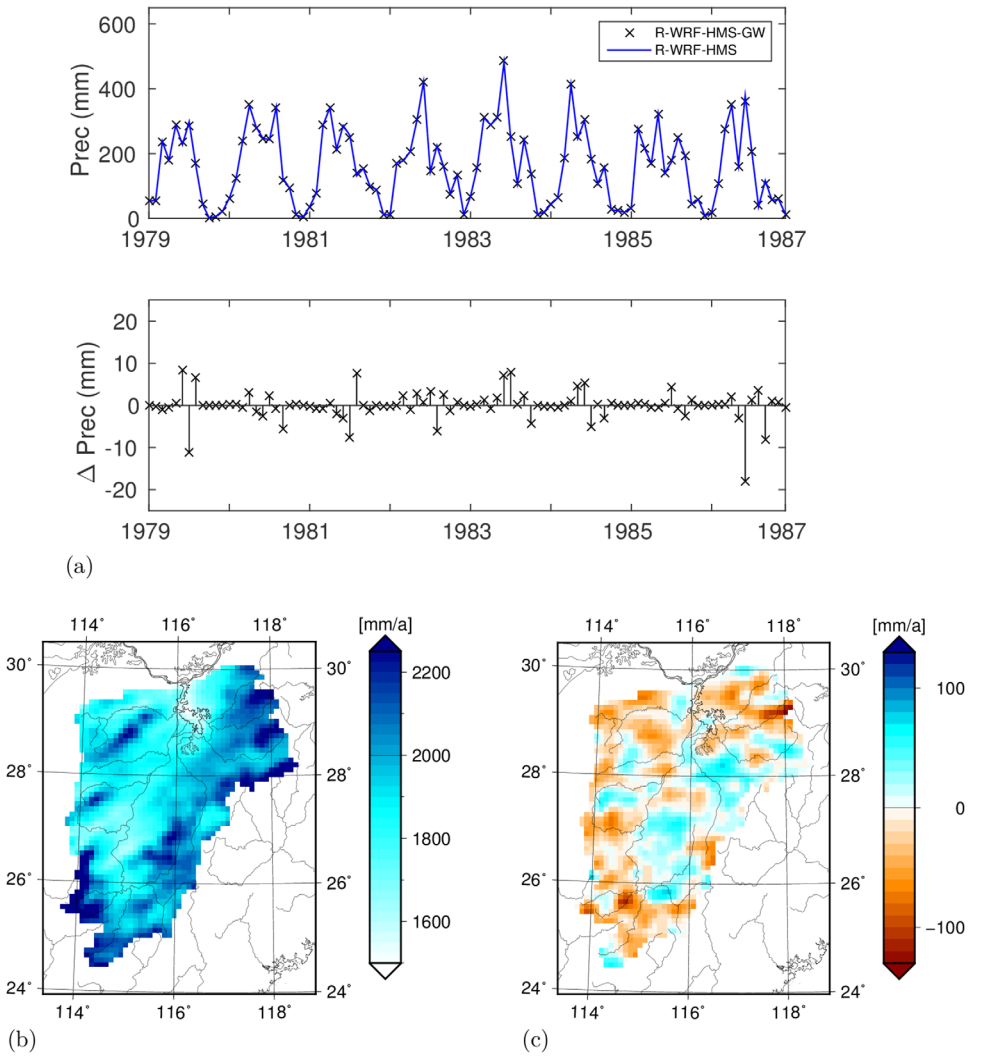

Figure 16. (a) Spatially averaged simulated monthly (top) precipitation and (bottom) differences of the fully coupled simulations R-WRF-HMS (blue) and R-WRF-HMS-GW (black); (b) spatial distribution of mean annual precipitation (mm) of R-WRF-HMS-GW and (c) corresponding mean annual differences (mm) compared to R-WRF-HMS for the Poyang Lake basin.

(see Table 2). In addition to CPC, evapotranspiration estimates of GLEAM [*Miralles et al*., 2011] are added to the comparison. These two products differ in particular in winter, where evapotranspiration amounts are below 5 mm (CPC) and around 30 mm (GLEAM). For the winter months, the simulated evapotranspiration amounts (approx. 30 mm) of the WRF simulations are comparable to GLEAM. WRF overestimates annual mean evapotranspiration by 46% (R-WRF-HMS) and 42% (R-WRF-HMS-GW) compared to the GLEAM product. The correlation coefficients of both simulations compared to GLEAM are 0.97.

For runoff, better performances are achieved with both simulations compared to CPC. The main differences occur during the dry period with underestimations in base flow which was already discussed in the streamflow analysis in section 4.4. Mean annual runoff is underestimated by 2% (R-WRF-HMS) and 16% (R-WRF-HMS-GW) compared to CPC. The correlation coefficients of both simulations with CPC are 0.88.

Basin averages of mean soil moisture of the first 1.6 m depth are shown in Figure 17c. Both simulation results are in general wetter compared to CPC, in particular, for the dry months. On average, mean soil moisture is 0.34 for R-WRF-HMS and 0.32 for R-WRF-HMS-GW compared to 0.30 for CPC. Correlation coefficients of both simulations with CPC are 0.85. The drier conditions of the fully coupled simulations with groundwater feedback are closer to the soil moisture estimations from CPC.

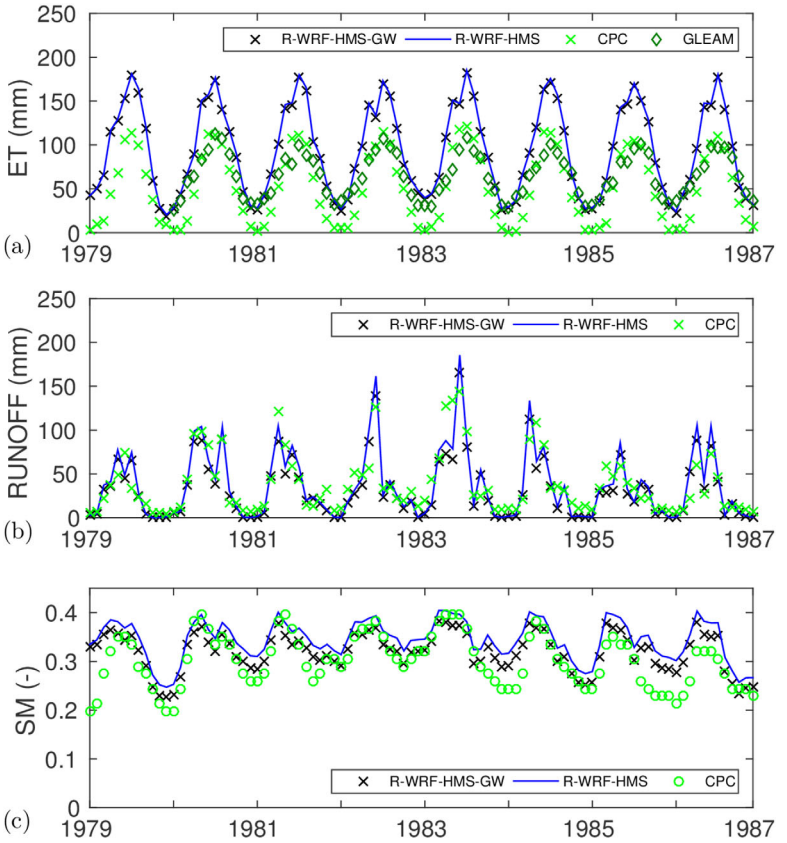

Figure 17. Spatially averaged simulated monthly (a) evapotranspiration, (b) surface runoff, and (c) soil moisture of the fully coupled simulations R-WRF-HMS (blue) and R-WRF-HMS-GW (black) evaluated against the CPC product (green) and GLEAM (darkgreen, evapotranspiration only) for the Poyang Lake basin.

5. Summary and Conclusions

In this study, we present the development and application of a fully coupled, mesoscale regional atmospheric-hydrologic modeling system, which allows in particular investigations of the long-term interactions between groundwater, the land surface, and the atmosphere. In our approach, the regional atmospheric model WRF-ARW is coupled with the hydrological model HMS using the Noah-LSM as intermediate link. In addition, two-way interaction between groundwater and the Noah-LSM is implemented by two approaches, the *Fixed-head* and *Darcy-flux* methods. Hence, in comparison to standard RCM simulations, the fully coupled model system enables lateral water flows at the surface and subsurface as well as two-way interaction between groundwater, the unsaturated zone, the land surface, and the atmosphere. The reasonable computational demand of this coupled model system allows regional, long-term simulations for climate-relevant scales of multiyears, and longer time periods.

The first application of the model system is performed for the Poyang Lake basin (160,000 km^2) in South China. At first, both models are applied in stand-alone mode for the study area. The stand-alone WRF simulation has a warm bias of 0.47°C and a wet bias between 21 and 26% compared to gridded validation data sets. The stand-alone HMS results driven by meteorological station data indicate reasonable performances in simulating streamflow for all tributaries of the Poyang Lake (monthly NSE values between 0.56 and 0.89) with generally better performance statistics with increasing catchment size.

The implementation of two-way interaction between groundwater and LSM results in spatially averaged larger recharge amounts and consequently, drier soil moisture conditions, and decreasing evapotranspiration and surface runoff amounts in this study. However, the results with enabled groundwater feedback depict the occurrence of upward fluxes in up to 27% of the basin area on monthly scale, showing a distinct annual cycle with a maximum coverage in December and January. Furthermore, the simulation

results indicate that there is a significant impact if two-way interaction between groundwater and unsaturated zone is implemented, but the differences between the two approaches *Fixed-head* and *Darcy-flux* are minor.

With the fully coupled atmospheric-hydrological model system, reasonable streamflow estimations in terms of seasonal cycle and inter-annual variability could be achieved. It is evident that the precipitation bias, mainly a wet bias, is transferred to the hydrological component of the modeling system. The impact of groundwater feedback on streamflow results is minor, because channel-groundwater interaction is comparatively low. These results indicate the significant impact of atmospheric simulation quality, in particular precipitation, on the hydrological part of the fully coupled modeling system. It is therefore of central importance that both parts, the atmospheric (WRF) and hydrological (HMS) model, provide reasonable results and are validated.

The impact of the fully coupled atmospheric-hydrological simulations on the terrestrial water balance indicates for spatial averages in general higher recharge amounts and consequently drier soil conditions and reduced evapotranspiration and surface runoff amounts with groundwater coupling in this study. However, groundwater coupling results in net recharge upward fluxes up to 25% of the basin area on monthly scale. The evaluation with the CPC and GLEAM products shows that soil moisture, evapotranspiration and surface runoff are overestimated by both simulations mainly due the overestimation of precipitation. With the implementation of groundwater feedback, simulation results for soil moisture and evaporation improve in comparison to the CPC and GLEAM products.

With the fully coupled model system, the changes in the land surface conditions also impact atmospheric variables. The overall annual mean temperature increase with groundwater feedback is 0.1°C. For precipitation, the overall impact of groundwater feedback is minor but temporal shifts and a spatial redistribution within the basin in the range of (±5%) occur.

To conclude, the results show that the developed fully coupled model system is able to simulate the atmospheric and hydrological conditions up to streamflow estimations in the rivers at regional and long-term time scales. The importance of groundwater coupling and its impact on land surface and atmospheric variables is demonstrated. For the Poyang Lake basin, a slight shift on the partitioning of surface turbulent fluxes with less latent heat flux and an increase of sensible heat flux is simulated considering groundwater feedback.

WRF-HMS enables a closed description of the water cycle at regional and long-term scale. This offers many further possible applications, including joint climate and land use change impact studies, to investigate hydro-meteorological flux responses at basin scale for different climate regions worldwide.

Acknowledgments

This research was supported financially by the German Research Foundation (DFG-grant KU 2090/2-1) and National Natural Science Foundation of China (grants 50909033 and 40911130507). Further we acknowledge support by the Helmholtz Regional Climate Initiative REKLIM. We appreciate the work and thank the following institutions for providing data: The European Centre for Medium-Range Weather Forecast for the reanalysis data ERA-Interim. The Earth Resources Observation and Science (EROS) from U.S. Geological Survey providing the HYDRO1k Elevation derivative database, which is available at https://lta.cr.usgs.gov/HYDRO1K. GPCP Precipitation and CPC data are provided by NOAA/OAR/ESRL PSD, Boulder, Colorado, USA, from their web site at http://www.esrl.noaa.gov/psd. The CRU precipitation and temperature data from the Climatic Research Unit, University of East Anglia, were downloaded from http://dx.doi.org/10.5285/D0E1585D-3417-485F-87AE-4FCECF10A99. The precipitation data from APHRODITE (Asian Precipitation - Highly-Resolved Observational Data Integration Towards Evaluation of Water Resources) were downloaded from http://www.chikyu.ac.jp/precip/index.html. We thank Miralles (University of Bristol) for kindly providing the GLEAM evapotranspiration data. The Chinese Geology Dataset was provided from State Key Laboratory of Resources and Environmental Information System, Institute of Geographic Sciences and Natural Resources Research, Chinese Academy of Sciences. The China Meteorological Administration provided meteorological station data and the Ministry of Water Resources of China streamflow data for the Poyang Lake basin. The simulations were carried out at the HPC cluster of KIT/IMK-IFU which uses the CentOS computing platform. Furthermore, we would like acknowledge the work of the developers of the data operators NCO and CDO. The fully coupled modeling system WRF-HMS is available from the authors upon request. We thank Martyn Clark and the three anonymous reviewers for their valuable comments.

References

Anyah, R., C. Weaver, G. Miguez-Macho, Y. Fan, and A. Robock (2008), Incorporating water table dynamics in climate modeling: 3. Simulated groundwater influence on coupled land-atmosphere variability, *J. Geophys. Res.*, *113*, D07103, doi:10.1029/2007JD009087.

Argüeso, D., J. Hidalgo-Muñoz, S. Gámiz-Fortis, M. Esteban-Parra, J. Dudhia, and Y. Castro-Díez (2011), Evaluation of WRF parameterizations for climate studies over Southern Spain using a multi-step regionalization, *J. Clim.*, *24*, 5633–5651.

Berg, P., S. Wagner, H. Kunstmann, and G. Schaedler (2013), High resolution regional climate model simulations for Germany: Part I-validation, *Clim. Dyn.*, *40*(1-2), 401–414, doi:10.1007/s00382-012-1508-8.

Betts, A., and M. Miller (1986), A new convective adjustment scheme. Part II: Single column tests using GATE wave, BOMEX, ATEX and arctic air-mass data sets, *Q. J. R. Meteorol. Soc.*, *112*(473), 693–709.

Betts, A. K. (1986), A new convective adjustment scheme. Part I: Observational and theoretical basis, *Q. J. R. Meteorol. Soc.*, *112*(473), 677–691.

Bogaart, P., A. Teuling, and P. Troch (2008), A state-dependent parameterization of saturated-unsaturated zone interaction, *Water Resour. Res.*, *44*, W11423, doi:10.1029/2007WR006487.

Butts, M., M. Drews, M. A. Larsen, S. Lerer, S. H. Rasmussen, J. Grooss, J. Overgaard, J. C. Refsgaard, O. B. Christensen, and J. H. Christensen (2014), Embedding complex hydrology in the regional climate system–dynamic coupling across different modelling domains, *Adv. Water Resour.*, *74*, 166–184.

Chen, F., and J. Dudhia (2001), Coupling an advanced land surface-hydrology model with the Penn State-NCAR MM5 modeling system. Part I: Model implementation and sensitivity, *Mon. Weather Rev.*, *129*(4), 569–585.

Clapp, R., and G. Hornberger (1978), Empirical equations for some soil hydraulic-properties, *Water Resour. Res.*, *14*(4), 601–604, doi:10.1029/WR014i004p00601.

Dee, D., et al. (2011), The ERA-Interim reanalysis: Configuration and performance of the data assimilation system, *Q. J. R. Meteorol. Soc.*, *137*(656), 553–597.

De Rooij, G. (2010), Comments on "Improving the numerical simulation of soil moisture-based Richards equation for land models with a deep or shallow water table", *J. Hydrometeorol.*, *11*, 1044–1050.

Dudhia, J. (1989), Numerical study of convection observed during the winter monsoon experiment using a mesoscale two-dimensional model, *J. Atmos. Sci.*, *46*(20), 3077–3107.
Fan, Y., and H. van den Dool (2004), Climate prediction center global monthly soil moisture data set at 0.5 resolution for 1948 to present, *J. Geophys. Res.*, *109*, D10102, doi:10.1029/2003JD004345.
Fersch, B., and H. Kunstmann (2014), Atmospheric and terrestrial water budgets: Sensitivity and performance of configurations and global driving data for long term continental scale WRF simulations, *Clim. Dyn.*, *42*(9-10), 2367–2396, doi:10.1007/s00382-013-1915-5.
Fersch, B., S. Wagner, T. Rummler, D. Gochis, and H. Kunstmann (2013), Impact of groundwater dynamics and soil-type on modelling coupled water exchange processes between land and atmosphere, *IAHS AISH Publ.*, *359*, 140–145.
Gochis, D., W. Yu, and D. Yates (2013), The WRF-Hydro model technical description and user's guide, version 1.0, NCAR Technical Document, pp. 1–120, Natl. Cent. for Atmos. Res., Boulder, Colo.
Guo, H., Q. Hu, and T. Jiang (2008), Annual and seasonal streamflow responses to climate and land-cover changes in the Poyang Lake basin, China, *J. Hydrol.*, *355*(1-4), 106–122, doi:10.1016/j.jhydrol.2008.03.020.
Hong, S., and J. Lim (2006), The WRF single-moment 6-class microphysics scheme (WSM6), *J. Korean Meteorol. Soc.*, *42*(2), 129–151.
Hong, S., J. Dudhia, and S. Chen (2004), A revised approach to ice microphysical processes for the bulk parameterization of clouds and precipitation, *Mon. Weather Rev.*, *132*(1), 103–120.
Hong, S., Y. Noh, and J. Dudhia (2006), A new vertical diffusion package with an explicit treatment of entrainment processes, *Mon. Weather Rev.*, *134*(9), 2318–2341.
Janjic, Z. I. (2000), Comments on ''Development and evaluation of a convection scheme for use in climate models'', *J. Atmos. Sci.*, *57*(21), 3686–3686.
Jiang, X., G.-Y. Niu, and Z.-L. Yang (2009), Impacts of vegetation and groundwater dynamics on warm season precipitation over the Central United States, *J. Geophys. Res.*, *114*, D06109, doi:10.1029/2008JD010756.
Kollet, S. J., and R. M. Maxwell (2008), Capturing the influence of groundwater dynamics on land surface processes using an integrated, distributed watershed model, *Water Resour. Res.*, *44*, W02402, doi:10.1029/2007WR006004.
Kondo, J., and J. Xu (1997), Seasonal variations in the heat and water balances for nonvegetated surfaces, *J. Appl. Meteorol.*, *36*(12), 1676–1695.
Larsen, M. A. D., J. C. Refsgaard, M. Drews, M. B. Butts, K. H. Jensen, J. Christensen, and O. Christensen (2014), Results from a full coupling of the HIRHAM regional climate model and the mike she hydrological model for a Danish catchment, *Hydrol. Earth Syst. Sci.*, *18*(11), 4733–4749.
Maxwell, R., and N. Miller (2005), Development of a coupled land surface and groundwater model, *J. Hydrometeorol.*, *6*(3), 233–247, doi:10.1175/JHM422.1.
Maxwell, R., J. Lundquist, J. Mirocha, S. Smith, C. Woodward, and A. Tompson (2011), Development of a coupled groundwater-atmosphere model, *Mon. Weather Rev.*, *139*(1), 96–116.
Maxwell, R. M., F. K. Chow, and S. J. Kollet (2007), The groundwater-land-surface-atmosphere connection: Soil moisture effects on the atmospheric boundary layer in fully-coupled simulations, *Adv. Water Resour.*, *30*(12), 2447–2466, doi:10.1016/j.advwatres.2007.05.018.
Miguez-Macho, G., Y. Fan, C. Weaver, R. Walko, and A. Robock (2007), Incorporating water table dynamics in climate modeling: 2. Formulation, validation, and soil moisture simulation, *J. Geophys. Res.*, *112*, D13108, doi:10.1029/2006JD008112.
Miralles, D., T. Holmes, R. De Jeu, J. Gash, A. Meesters, and A. Dolman (2011), Global land-surface evaporation estimated from satellite-based observations, *Hydrol. Earth Syst. Sci.*, *15*(2), 453–469.
Mitchell, T., and P. Jones (2005), An improved method of constructing a database of monthly climate observations and associated high-resolution grids, *Int. J. Climatol.*, *25*(6), 693–712, doi:10.1002/joc.1181.
Mlawer, E., S. Taubman, P. Brown, M. Iacono, and S. Clough (1997), Radiative transfer for inhomogeneous atmospheres: RRTM, a validated correlated-k model for the longwave, *J. Geophys. Res.*, *102*(D14), 16,663–16,682.
Niu, G.-Y., Z.-L. Yang, R. E. Dickinson, L. E. Gulden, and H. Su (2007), Development of a simple groundwater model for use in climate models and evaluation with gravity recovery and climate experiment data, *J. Geophys. Res.*, *112*, D07103, doi:10.1029/2006JD007522.
Rosero, E., Z.-L. Yang, L. E. Gulden, G.-Y. Niu, and D. J. Gochis (2009), Evaluating enhanced hydrological representations in NOAH LSM over transition zones: Implications for model development, *J. Hydrometeorol.*, *10*(3), 600–622.
Schneider, U., A. Becker, P. Finger, A. Meyer-Christoffer, B. Rudolf, and M. Ziese (2011), GPCC full data reanalysis version 6.0 at 0.5°: Monthly land-surface precipitation from rain-gauges built on GTS-based and historic data, Global Precipitation Climatology Centre status report, Global Precipitation Climatol. Cent., Offenbach, Germany, doi:10.5676/DWD_GPCC/FD_M_V6_050.
Seuffert, G., P. Gross, C. Simmer, and E. Wood (2002), The influence of hydrologic modeling on the predicted local weather: Two-way coupling of a mesoscale weather prediction model and a land surface hydrologic model, *J. Hydrometeorol.*, *3*(5), 505–523.
Shankman, D., B. D. Keim, and J. Song (2006), Flood frequency in China's Poyang Lake region: Trends and teleconnections, *Int. J. Climatol.*, *26*(9), 1255–1266, doi:10.1002/joc.1307.
Shrestha, P., M. Sulis, M. Masbou, S. Kollet, and C. Simmer (2014), A scale-consistent terrestrial systems modeling platform based on COSMO, CLM, and Parflow, *Mon. Weather Rev.*, *142*(9), 3466–3483.
Skamarock, W., J. Klemp, J. Dudhia, D. Gill, D. Barker, M. Duda, X. Huang, W. Wang, and J. Powers (2008), A description of the Advanced Research WRF version 3, *NCAR Tech. Note 475*, Natl. Cent. for Atmos. Res., Boulder, Colo.
Wagner, S., B. Fersch, H. Kunstmann, F. Yuan, C. Yang, and Z. Yu (2013), Hydrometeorological modelling for Poyang Lake region, China, *IAHS AISH Publ.*, *359*, 152–157.
Wei, J., H. R. Knoche, and H. Kunstmann (2015), Contribution of transpiration and evaporation to precipitation: An ET-Tagging study for the Poyang Lake region in Southeast China, *J. Geophys. Res. Atmos.*, *120*, 6845–6864, doi:10.1002/2014JD022975.
Yatagai, A., K. Kamiguchi, O. Arakawa, A. Hamada, N. Yasutomi, and A. Kitoh (2012), APHRODITE constructing a long-term daily gridded precipitation dataset for Asia based on a dense network of rain gauges, *Bull. Am. Meteorol. Soc.*, *93*(9), 1401–1415, doi:10.1175/BAMS-D-11-00122.1.
Ye, X., Q. Zhang, J. Liu, X. Li, and C.-Y. Xu (2013), Distinguishing the relative impacts of climate change and human activities on variation of streamflow in the Poyang Lake catchment, China, *J. Hydrol.*, *494*, 83–95, doi:10.1016/j.jhydrol.2013.04.036.
Yeh, P., and E. Eltahir (2005), Representation of water table dynamics in a land surface scheme. Part I: Model development, *J. Clim.*, *18*(12), 1861–1880, doi:10.1175/JCLI3330.1.
York, J. P., M. Person, W. J. Gutowski, and T. C. Winter (2002), Putting aquifers into atmospheric simulation models: An example from the mill creek watershed, northeastern kansas, *Adv. Water Resour.*, *25*(2), 221–238, doi:10.1016/S0309-1708(01)00021-5.
Yu, Z., D. Pollard, and L. Cheng (2006), On continental-scale hydrologic simulations with a coupled hydrologic model, *J. Hydrol.*, *331*(1), 110–124.
Yuan, X., Z. Xie, J. Zheng, X. Tian, and Z. Yang (2008), Effects of water table dynamics on regional climate: A case study over East Asian monsoon area, *J. Geophys. Res.*, *113*, D21112, doi:10.1029/2008JD010180.

Yuan, F., H. Kunstmann, C. Yang, Z. Yu, L. Ren, B. Fersch, and Z. Xie (2009), Development of a coupled land-surface and hydrology model system for mesoscale hydrometeorological simulations, *IAHS Publ.*, *333*, 195–202.

Zeng, X., and M. Decker (2009), Improving the numerical solution of soil moisture-based Richards equation for land models with a deep or shallow water table, *J. Hydrometeorol.*, *10*(1), 308–319.

Zhang, Q., X.-C. Ye, A. D. Werner, Y.-L. Li, J. Yao, X.-H. Li, and C.-Y. Xu (2014), An investigation of enhanced recessions in Poyang Lake: Comparison of Yangtze River and local catchment impacts, *J. Hydrol.*, *517*, 425–434, doi:10.1016/j.jhydrol.2014.05.051.